Supporting Information

Designing of UiO-66 Based Super Protonic Conductor with the Highest MOF Based Proton Conductivity

Subhabrata Mukhopadhyay, Joyashish Debgupta, Chandani Singh, Rudraditya Sarkar, Olivia Basu, Samar K. Das*
E-mail: skdas@uohyd.ac.in; samar439@gmail.com
School of Chemistry, University of Hyderabad, Hyderabad – 500046, India

Table of Contents:

Section S1.	Physical Measurements	S-2
Section S2.	Synthesis, material and procedures	S-2→S-3
Section S3.	PXRD pattern of UiO-66-NH_2, **PSM 1** and **PSM 2**	S-3
Section S4.	TGA of UiO-66-NH_2, **PSM 1** and **PSM 2**	S-4
Section S5.	FT-IR and UV-Vis. spectral analysis of UiO -66-NH_2, **PSM 1** and **PSM 2**	S-4→S-5
Section S6.	Stability check of **PSM 1** and **PSM 2** under harsh conditions	S-5→S-6
Section S7.	(a) FESEM and EDX Analysis of **PSM 1** and **PSM 2** (b) Particle size of **PSM 1** and **PSM 2** from FESEM and DLS	S-5→S-8
Section S8.	Elemental analysis of **PSM 1** and **PSM 2** from ICP-AES analysis and determination of extent of post synthetic modification in each.	S-8→S-9
Section S9.	Gas sorption analysis of UiO-66-NH_2, **PSM 1** and **PSM 2**	S-9→S-10
Section S10	(a)Water sorption analysis of UiO-66-NH_2, **PSM 1** and **PSM 2**. (b) Calculation of water sorption per S atom.	S-10→S-11
Section S11	XPS analysis of **PSM 1** and **PSM 2** and UiO-66-NH_2.	S-11
Section S12	Digestive NMR and ESI-MS analysis of **PSM 1** and **PSM 2**	S-11→S-13
Section S13	Impedance spectroscopic analysis (a) General methodology and set up of measurement (b) Proton conductivity measurement under various relative humidity. (c) Proton conductivity measurement under different temperature. (d) Conductivity of Lithiated **PSM 1** (e) Calculation of proton conductivity from Impedance spectra by fitting with equivalent circuit	S-13→S-22
Section S14	Long term stability under operational condition.	S-22→S-24
Section S15	Activation energy calculation	S-24→S-25
Section S16	Computational details of ground energy minimized structures of model systems of **PSM 1**, **PSM 2** and UiO-66-NH_2.	S-25 →S-31
Section S17	Theoretical pK_a calculation of model compounds.	S-32
Section S18	NBO analysis on model compounds of **PSM 1** and **PSM 2**	S-33
Section S19	Tabular representation of various reported MOF based proton conductors and their conductivities	S-34
	References	S-35

Section S1. Physical Measurements

The synthesized compounds were characterized by powder X-ray diffraction, FT-IR, Gas adsorption analysis, FESEM imaging techniques, Thermogravimetry (TGA) and Impedance spectroscopy.

Infra-red spectra of solid samples were obtained as KBr pellets on a JASCO–5300 FT–IR spectrophotometer. Diffuse Reflectance (DRS) UV-Vis spectra were recorded using Shimadzu-2600 spctrophotometer. Thermogravimetric (TGA) analyses were carried out on a STA 409 PC analyzer. Field emission Scanning Electron Microscope (FE-SEM) imaging with energy dispersive X-ray (EDX) spectroscopy was carried out on a Carl Zeiss model Ultra 55 microscope: EDX spectra and maps were recorded using Oxford Instruments X-Max^N SDD (50 mm^2) system and INCA analysis software. All impedance measurements were conducted using a Zahner Zanium electrochemical work station operated with Thales software.

Section S2. Synthesis, Material and Synthetic procedures:

Synthesis of UiO-66-NH_2:

Synthesis of UiO-66-NH_2 was adapted from the works of Farha and coworkers.[1] UiO-66-NH_2 MOF was prepared using 5.4 mmol of $ZrCl_4$, which was dissolved in 50 mL DMF in presence of 10 mL conc. HCl by sonication. Then 6.75 mmol. BDC-NH_2 was added along with 100 mL of DMF. The reaction mixture was kept at 80 °C temperature for 24 hours in a sealed Teflon capped container. After slow cooling over a period of 6 hours the reaction mixture was filtered and washed. Next, the crude UiO-66-NH_2 was stirred in dry ethanol for 72 hours to remove absorbed DMF molecules prior to further characterizations.

Synthesis of PSM 1 and PSM 2:

Fully activated and characterized UiO-66-NH_2 were subjected to post synthetic modification. Earlier, Yaghi and coworkers[2] performed ring opening reactions of 1, 3 propane sultone with IRMOF-3. Similar reactions were later performed successfully with other MOF systems. Similar reaction scheme was used to prepare **PSM 1** and **PSM 2** from UiO-66. Freshly prepared and purified UiO-66-NH_2 was treated with 1, 3-Propane Sultone and 1,4-Butane Sultone separately in presence of DCM as solvent at room temperature for a period of 24 hours. UiO-66-NH_2 and sultone were taken in such a manner that the reaction mixture had sultone in equivalent amount to that of NH_2 groups of UiO-66-NH_2 framework. After 24 hours the post synthetically modified compounds

were filtered and repeatedly washed with DCM, water and ethanol to get rid of any unreacted and trapped sultone/ hydrolyzed sulfonic acid from the pores. Finally the post synthetically modified compounds were subjected to further studies.

Synthesis of PSM 1-Li:

PSM 1-Li was prepared by ion exchange between the labile protons of Brönsted acid group of **PSM 1** and Li^+ ion. The ion exchange was performed by stirring **PSM 1** in 0.5 M aqueous solution of LiCl for 72 hours. The modified compound i.e., **PSM 1**-Li was washed thoroughly after the completion of ion exchange so that unreacted LiCl trapped inside the channels of UiO-66 framework can be eliminated.

Section S3. PXRD pattern of PSM 1-Li:

Comparison of PXRD pattern of **PSM 1**-Li with the simulated pattern of UiO-66 suggests that structural integrity of the UiO-66 framework is retained in **PSM 1**-Li as well (Figure S1).

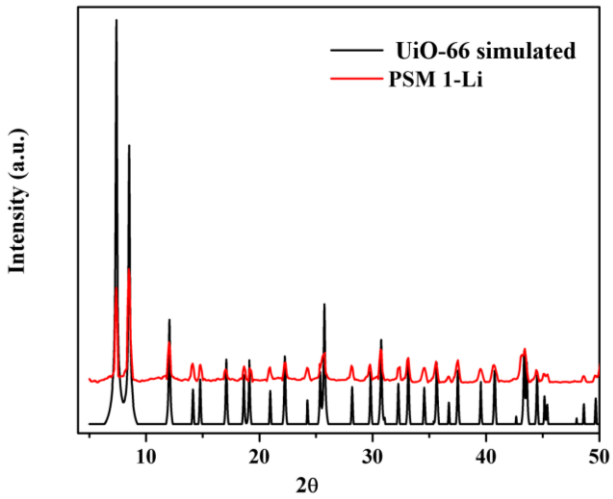

Figure S1. PXRD pattern of **PSM 1**-Li compared with simulated pattern of UiO-66.

Section S4. TGA of UiO-66-NH_2, PSM 1 and PSM 2:

Thermogravimetric analysis (Figure S2) of UiO-66-NH_2, **PSM 1** and **PSM 2** were carried under aerial atmosphere without preactivation of any of the compounds. All the three compounds followed a similar trend and lost ~20% of its initial weight within 180 °C. Absorbed volatile molecules were evaporated in this region. From 200 °C **PSM 1** and **PSM 2** followed a steeper slope than that of UiO-66-NH_2. This might be due to oxidation of the pendant alkyl chain and $–SO_3H$ group of these two compounds unlike that of UiO-66-NH_2. Around 400 °C significant weight loss was observed for all the three compounds due to structural changes in the framework structure. It is well-established fact that, in this region of temperature the ‘Zr-OH’ functionalization of the metal node gets converted to ‘Zr=O’ while

losing water. Complete disintegration of UiO-66 framework takes place around 600 °C temperature. In higher temperature the residual compound completely converts into oxides. As a result, the residual mass of ~17% is composed of zirconium oxides in all the three compounds.

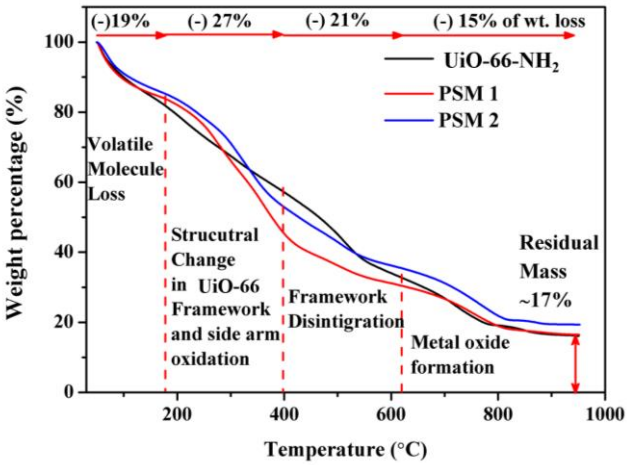

Figure S2. TG analysis of UiO-66-NH_2, **PSM 1** and **PSM 2** under aerial atmosphere.

Section S5. UV-Vis. spectral analysis of UiO-66-NH_2, PSM 1 and PSM 2

Diffused reflectance UV-Vis. spectra were recorded and Kubelka-Munk converted for all the three compounds in their solid state (refer to Figure S3). λ_{max} of UiO-66-NH_2 was found to be little red shifted in **PSM 1** and **PSM 2** as a result of '–SO_3H' attachment *via* post synthetic modification.

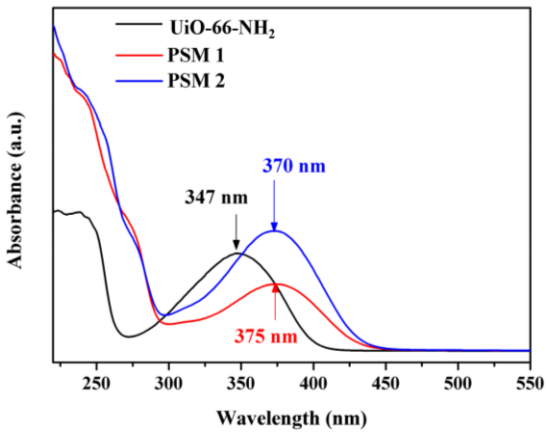

Figure S3. UV-Vis DR spectra of UiO-66-NH_2 (or PCM 8), **PSM 1** and **PSM 2** recorded in solid state.

Section S6. Stability check of PSM 1 and PSM 2 under harsh conditions:

To investigate the stability issues with the two post synthetically modified compounds i.e., **PSM 1** and **PSM 2** were subjected to various harsh conditions e.g., (a) kept in open air for one year, (b) stored in water for more than one month (c) treated with boiling water for 1 week and (d) kept under 6 ton pressure for 1 hour. After each of the experiment PXRD pattern was recorded and compared with the simulated pattern of UiO-66. No notable change

could be observed in any of the cases in peak positions (Figure S4 and Figure S5). This suggests **PSM 1** and **PSM 2** to retain its basic framework structure under high pressure conditions, prolonged aqueous (boiling water) treatment and also confirms their aerial stability. All these factors are crucial for a probable application in designing of proton conducting membrane in fuel cell.

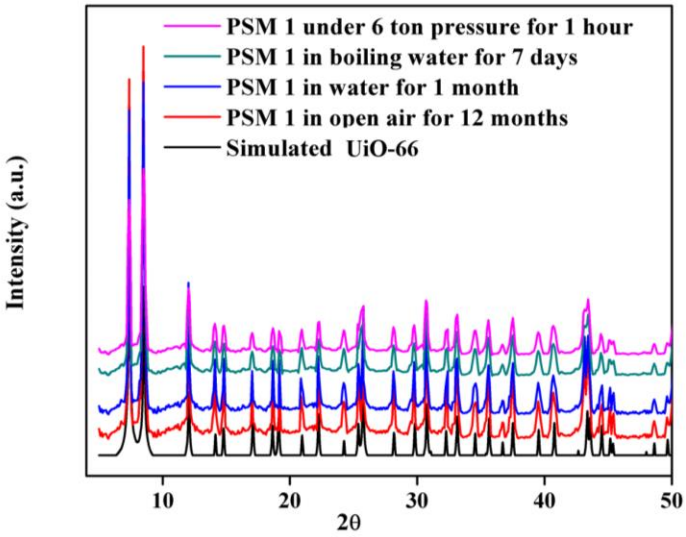

Figure S4. PXRD pattern of **PSM 1** under various harsh conditions.

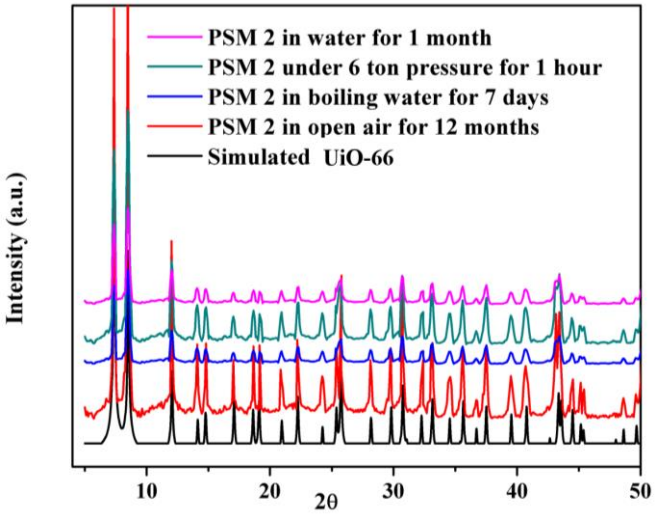

Figure S5. PXRD pattern of **PSM 2** under various harsh conditions.

Section S7. (a) FESEM and EDX Analysis of PSM 1 and PSM 2:

FESEM images were recorded for both **PSM 1** and **PSM 2**. No specific morphology was observed in either case. (Figure S6)

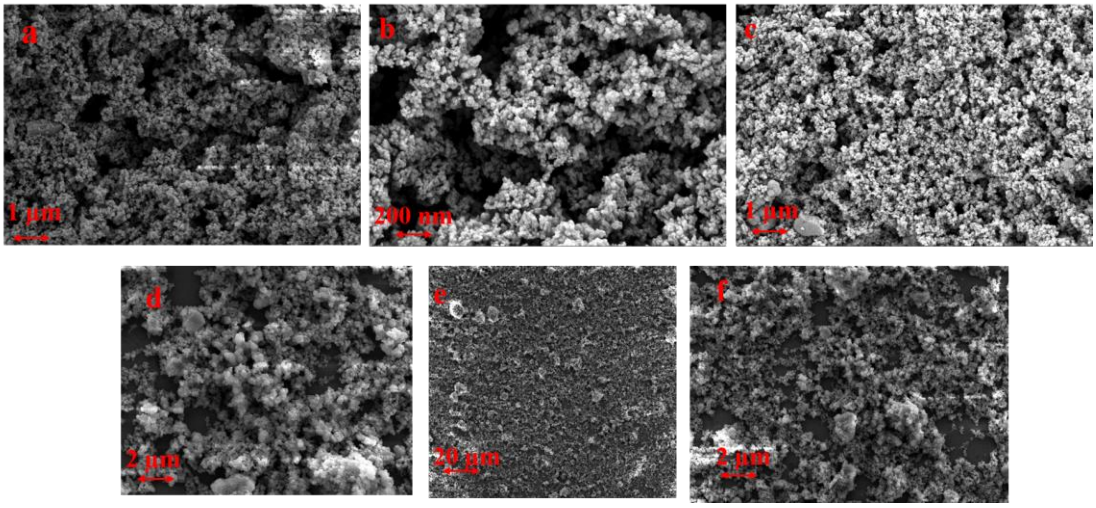

Figure S6. FESEM images of **PSM 1** (a to c) and **PSM 2**(d to f).

We also recorded FESEM images (Figure S7) and EDX-profile (Figure S8) of pelletized sample of **PSM 1**. The FESEM image clearly shows the face of the pellet to be covered with carbon paper while sides of the pellet were uncovered. Morphology of the pellet cross section was analysed by EDX analysis and found to infer the same observation as earlier.

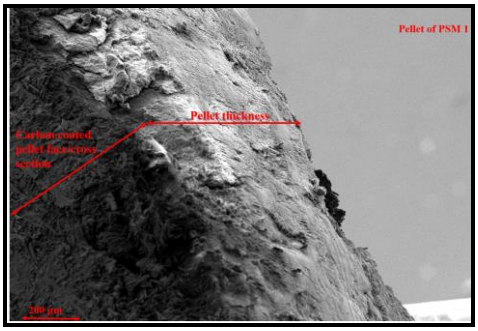

Figure S7. FESEM image of the edge of the pellet of **PSM 1** showing the thickness of the pellet.

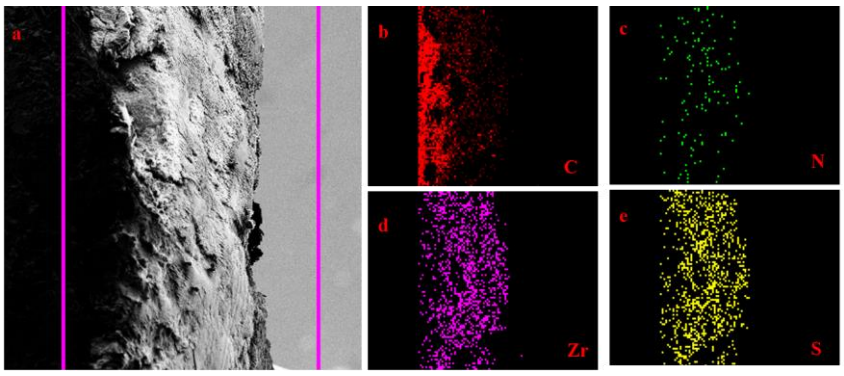

Figure S8. EDX analysis of pellet of **PSM 1** showing elemental distribution around the edge of the pellet.

(b) Size distribution of PSM 1 and PSM 2 from FESEM and DLS measurements:

The particle size of **PSM 1** and **PSM 2** was examined through FESEM analysis. FESEM images were recorded with same magnification for both **PSM 1** and **PSM 2**. As it is evident

from Figure S9 that, 100 nm ≤ diameter of particle ≤ 200 nm for majority of **PSM 1** and also **PSM 2**. Thus, the particle sizes can be considered to be similar in both the cases.

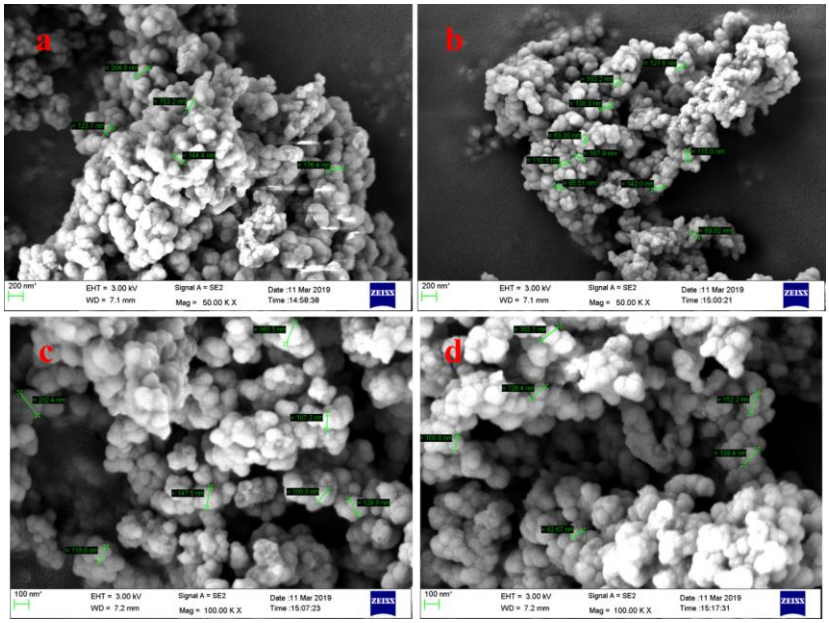

Figure S9. (a)&(b) FESEM images at 200 nm scale of **PSM 1** and **PSM 2** respectively. (c)&(d) FESEM images of **PSM 1** and **PSM 2** at 100 nm scale. Particle size distribution of 100 nm ≤ diameter of particle ≤ 200 nm can be observed for **PSM 1** and **PSM 2**.

DLS (dynamic light scattering) measurements for **PSM 1** and **PSM 2** were also carried out. **PSM 1** and **PSM 2** were dispersed in methanol for DLS measurement. Hydrodynamic diameter of **PSM 1** was found to be 220.2 nm and that of **PSM 2** was 255.0 nm; the polydispersity index was 0.21 and 0.23 for **PSM 1** and **PSM 2** respectively. Similar radius and narrow size distribution was observed from DLS measurement (Figure S10).

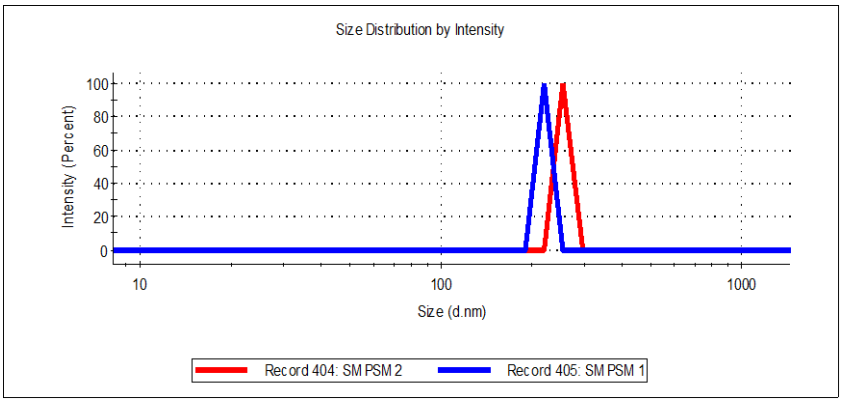

Figure S10. DLS spectra of **PSM 1** and **PSM 2** dispersed in methanol.

From the particle size analysis of **PSM 1** and **PSM 2** by FESEM and DLS measurement, it can be said that, the difference in proton conductivity of **PSM 1** and **PSM 2** is not a result of difference in particle sizes of both.

Section S8. Elemental analysis of PSM 1 and PSM 2 from ICP-AES analysis and determination of extent of post synthetic modification in each:

To understand the extent of post synthetic modification, inductively coupled plasma atomic emission spectroscopy was performed for the element sulfur and Zirconium in **PSM 1** and **PSM 2**. From the analysis, a mere 5.02% (w/w) and 5.03% (w/w) of sulfur content was found for **PSM 1** and **PSM 2** respectively. Repeat experiments gave similar data and proved the homogeneity of sample, while Zr : S ratio was found to be ≈ 5:1, (w/w) in both **PSM 1** and **PSM 2** (Table S1 and S2). Similar loading of sulfur in **PSM 1** and **PSM 2** also confirms similar extent of post synthetic modification in both the compounds.

Calculation from ICP AES analysis and molecular formula of UiO-66-NH_2:

Unit cell formula of UiO-66-NH_2: $Zr_{24}O_{120}C_{192}H_{96}N_{24}$

Molar mass of UiO-66-NH_2: 6848.3064.

Thus, most accurate formula of **PSM 1**: $\mathbf{Zr_{24}O_{120}C_{192}H_{83}N_{24}(C_3H_6O_3S)_{13}}$; calculated weight percent of sulfur is 4.94%, while calculated Zr: S ≈ 5:1 (w/w) (approx.).

Thus, most accurate formula of **PSM 2**: $\mathbf{Zr_{24}O_{120}C_{192}H_{83}N_{24}(C_4H_8O_3S)_{14}}$; (calculated weight percent of sulfur is 5.1% while calculated Zr: S ≈ 5:1 (w/w) (approx.) respectively.

According to the empirical formula mentioned above, the ratio of Zr : [($C_3H_6O_3S$) or ($C_4H_8O_3S$)] is 2:1 (approx.) in both the post synthetically modified compounds.

The result obtained so far suggests that, nearly half of the '-NH_2' groups are post synthetically modified in both the compounds and remaining half are still free.

Table S1. ICP-AES analysis data of PSM 1:

Sample Particulars: PSM-1

Qty. Received: 100mg X 1no Plastic Vial

Test Parameters: Sulfur as S and Zirconium as Zr

Date of Receipt of Sample : 14/09/2017 **Date of Starting of Analysis:** 21/09/2017

Date of completion of analysis: 23/09/2017 *SAMPLE TESTED AS RECEIVED*

TEST RESULTS

S.No.	Parameters	UOM	Results
1	Sulfur as S	% by mass	5.02
2.	Zirconium as Zr	% by mass	25.98

Instrument Used: ICP-OES Varian 720-ES

NOTE: This report and results relate only to the sample / items tested.

Table S2. ICP-AES analysis data of PSM 2:

Sample Particulars: PSM-2

Qty. Received: 100mg X 1no Plastic Vial

Test Parameters: Sulfur as S and Zirconium as Zr

Date of Receipt of Sample : 14/09/2017 Date of Starting of Analysis: 21/09/2017

Date of completion of analysis: 23/09/2017 *SAMPLE TESTED AS RECEIVED*

TEST RESULTS

S.No.	Parameters	UOM	Results
1	Sulfur as S	% by mass	5.03
2.	Zirconium as Zr	% by mass	25.92

Instrument Used: ICP-OES Varian 720-ES

NOTE: This report and results relate only to the sample / items tested.

Section S9. Gas sorption analysis of UiO-66-NH_2, PSM 1 and PSM 2:

To evaluate the effect of post synthetic modification on the porosity of UiO-66-NH_2, N_2 sorption measurement has been carried out on UiO-66-NH_2 as well as on the two post synthetically modified compounds. Prior to gas sorption studies UiO-66-NH_2, **PSM 1** and **PSM 2** were activated by degassing for 6 hours in 140 °C temperature. All the three compounds showed Type-I isotherm indicating the presence of micropores inside. However, surface area (calculated using Brunauer–Emmett–Teller method) of UiO-66-NH_2 was found to be ~370 m^2g^{-1} higher than that of **PSM 1** and **PSM 2**. It was expected due to the presence of bulky alkyl chain inside the cavity of **PSM 1** and **PSM 2**, which causes a lowering of available surface area and pore volume for sorption of N_2. Furthermore, **PSM 2** was observed to have a lower surface area than that of **PSM 1**. This can be a result of two factors i.e., (1) longer alkyl chain of side arm of **PSM 2** than **PSM 1**; and (2) the minute higher loading of alkyl chain containing '-SO_3H' group in case of **PSM 2** when compared with **PSM 1**. Thus, it can be said that, in this case, the N_2 sorption analysis served as a very convincing tool to establish the successful post synthetic modification in case of **PSM 1** and **PSM 2**.

It is important to mention that, the observed BET surface area of the pristine UiO-66-NH_2 was lower than that of similar systems (i.e., UiO-66-NH_2) reported in recent times. This lower BET surface area was not a result of less crystalline nature of the pristine UiO-66-NH_2 but was due to activation (degassing) at relatively low temperature. To confirm this, further N_2 sorption analysis (Figure S11) was carried out on pristine UiO-66-NH_2 microcrystals after activating them through degassing at 180 °C for 12 hours. This later

analysis shows a BET surface area of 1086 m^2/g for pristine UiO-66-NH_2 which matches well with the reported ones in the literature. Thus, the as synthesized parent MOF *i.e.*, UiO-66-NH_2 is highly crystalline in nature and shows properties similar to the earlier reports on UiO-66-NH_2 systems.

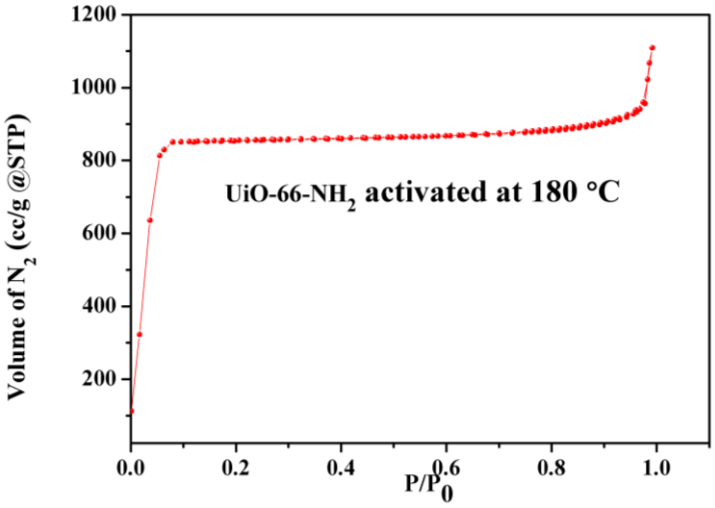

Figure S11. N_2 sorption isotherm of UiO-66-NH_2, activated at 180 °C prior to analysis.

Section S10. (a) Water adsorption analysis of UiO-66-NH_2, PSM 1 and PSM 2:

Water sorptivity plays a very crucial role for water assisted proton conduction. Thus, water sorptivity was measured for all the three compounds *i.e.*, UiO-66-NH_2, **PSM 1** and **PSM 2**. Prior to measurement, all the three compounds were activated at 140 °C for 6 hours.

(b) Determination of water uptake per S atom in case of PSM 1 and PSM 2 from water sorption measurement:

The calculation of water uptake per S atom in case of **PSM 1** and **PSM 2** was done from water sorption analysis. Measurement was conducted at 25 °C. A known amount of sample was kept at increasing relative humidity (P/P_0) to maximum relative humidity (RH_{max}) of 90%. The volume of water sorption (at STP) with increase in relative humidity as a result of increased water sorption was measured.

Calculation for PSM 1:

Volume of water sorption at ($P/P_0 = 0.9$) is: 310 cc

Thus, 1 mole of **PSM 1** adsorbs (310× 8423)/(22400) mole of water.

Each molecular unit of **PSM 1** has 13 S atoms. Please see the calculation of molecular weight of **PSM 1** and **PSM 2** given above.

Thus, water sorption per S atom for **PSM 1** is ≈ 9.

Calculation for PSM 2:

Volume of water sorption at ($P/P_0 = 0.9$) is: 350 cc

Thus, 1 mole of **PSM 2** adsorbs (350× 8741.55)/(22400) mole of water.

Each molecular unit of **PSM 1** has 14 S atoms. Please see the calculation of molecular weight of **PSM 1** and **PSM 2** given above.

Thus, water sorption per S atom for **PSM 1** is ≈ 9.5.

Section S11: XPS analysis of UiO-66-NH_2, PSM 1 and PSM 2

X-ray photoelectron microscopy was carried out using ESCA+, (omicron nanotechnology, Oxford Instrument Germany) equipped with monochromator Aluminum Source (Al k_α radiation hυ =1486.7eV). The instrument was operated at 15 kV and 20mA. Pass energy for short scan was 20eV and in case of survey it was 50eV. Sample were taken in powder form, and deposited on Cu tape and degassed for overnight in XPS FEL chamber to minimize the air contaminator at sample surface. To overcome the charging problem a charge neutralizer of 2 keV is applied and binding energy of C1s core (284.6eV) was taken as reference. Angle between analyser to source was 90°.

Both **PSM 1** and **PSM 2** showed N1s binding energy (BE) characteristic of primary amine and also secondary amine while N1s binding energy for UiO-66-NH_2 shows peak for only primary amine. Careful analysis of N1s X-ray photoelectron spectra shows that, **(BE N1s of secondary amine)$_{PSM\ 2}$ < (BE N1s of secondary amine)$_{PSM\ 1}$.**The higher binding energy of secondary amine ('-NH-CH_2-CH_2-CH_2-SO_3H) of **PSM 1** by 0.2 eV suggests a drift of electron density towards nitrogen from the attached alkyl chain containing pendant '-SO_3H' group, which ultimately can result into increased acidity (i.e., lower pK_a) of **PSM 1** in comparison to **PSM 2**. The enhancement of acidity of **PSM 1** played a crucial role in enhancing its proton conductivity.

On the other hand, $S2p_{3/2}$ X-ray photoelectron spectra shows binding energy of sulphur at ~168.3 eV for both **PSM 1** and **PSM 2**, indicating the presence of sulphur in +IV oxidation state in both the compounds.

Section S12. Digestive NMR analysis of PSM 1 and PSM 2:

PSM 1 and **PSM 2** were digested in HF and dried over a period of one week. The dried powdered materials were analyzed by ^1H and ESI-MS analysis. Due to variety of fragmentation under prolonged HF treatment ^1H NMR and ESI-MS spectra of **PSM 1** and **PSM 2** contained lots of peaks due to impurity, but the characteristic peaks of the compounds were also observed. In ^1H NMR spectra (Figure S12 and Figure S13) of digested **PSM 1** and **PSM 2** peaks due to alkyl chain and aromatic benzene ring were present.

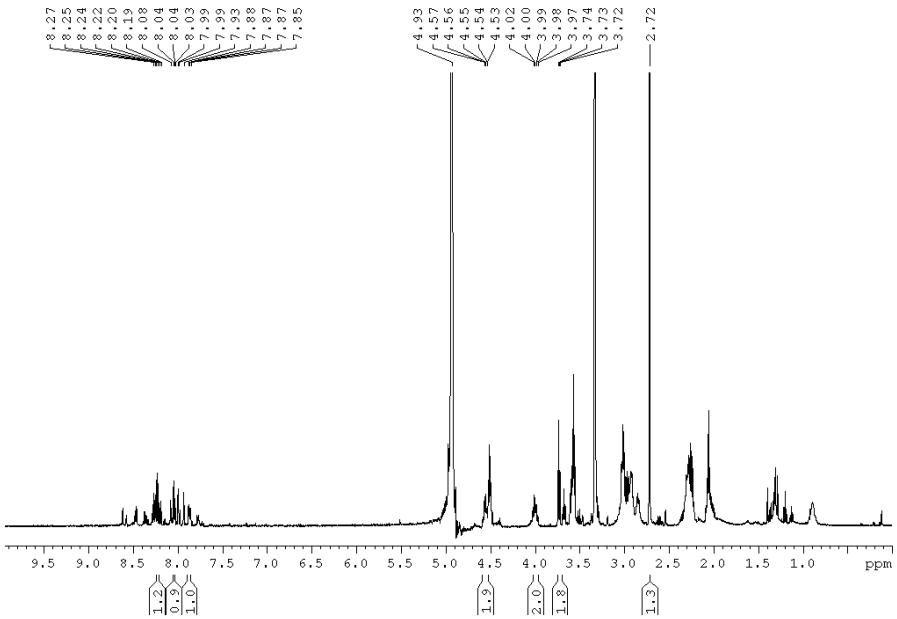

Figure S12. [1]H NMR spectrum of digested sample of **PSM 1**.

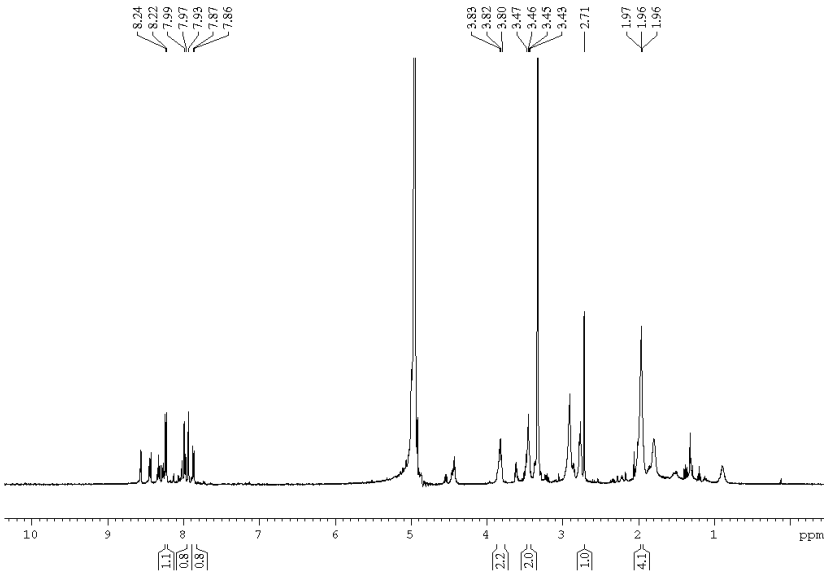

Figure S13. [1]H NMR spectrum of digested sample of **PSM 2**.

On the other hand, the ESI-MS spectrum of digested sample of **PSM 1** (Figure S14) showed high intensity peak at m/z value of 303.48 while in case of **PSM 2** (Figure S15) the high intense peak was observed at m/z value of 317.02. The peak positions were matching with the expected structures of the fragments of **PSM 1** and **PSM 2**. Samples were dissolved in methanol for ESI-MS studies.

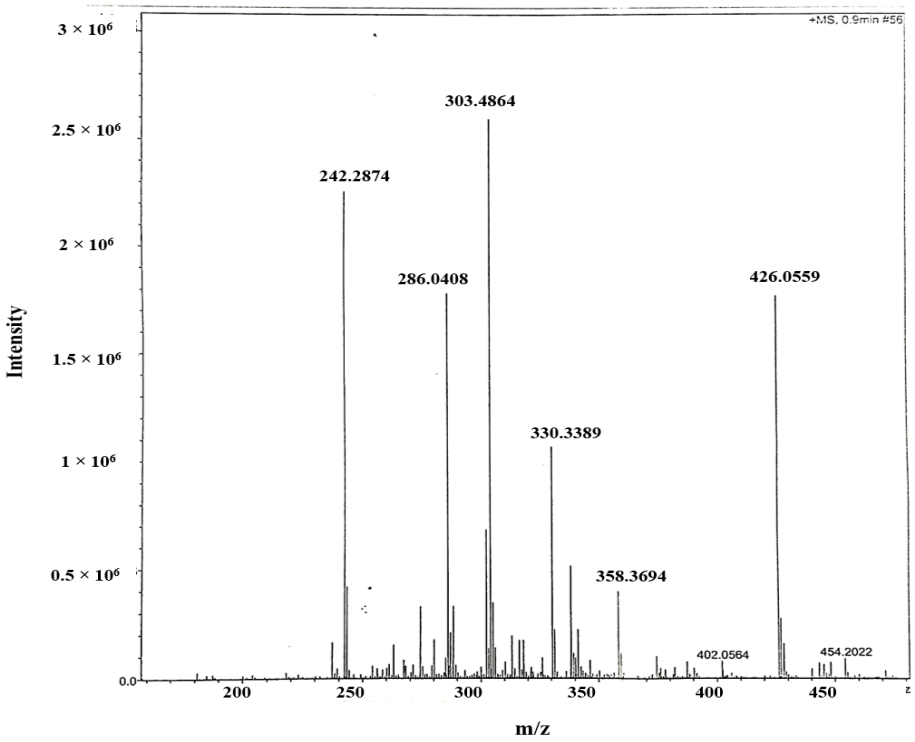

Figure S14. ESI-MS spectrum of digested sample of **PSM 1**.

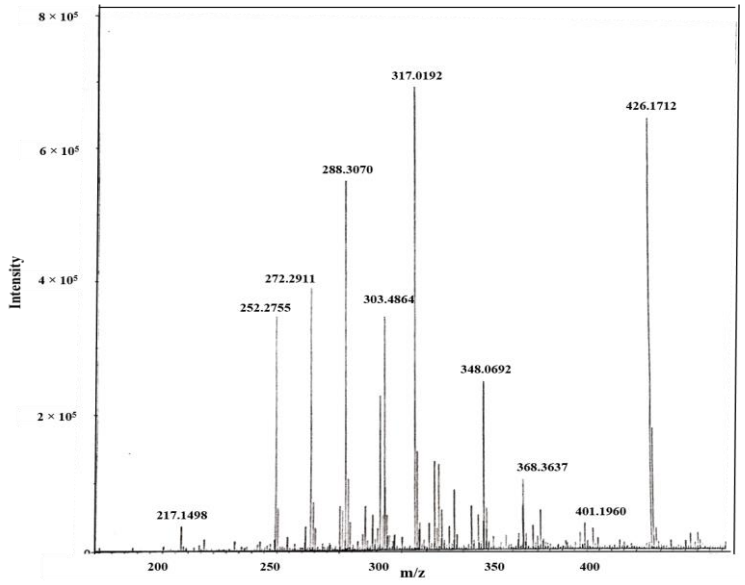

Figure S15. ESI-MS spectrum of digested sample of **PSM 2**.

Section S13. Impedance spectroscopic analysis:

(a) General methodology and set up of measurement:

Impedance measurement was performed using 2-electrode direct measurement method. Sample was taken as pellet for conductivity measurements.

Sample preparation:

Both the compounds *i.e.*, **PSM 1** and **PSM 2** were pelletized using similar protocol. To prepare the pellets, 400 mg of powdered sample was sandwiched between two carbon papers and kept under a hydraulic pressure of 5 ton for 3 minutes. Here the carbon papers were used to lower the contact resistance between the pellet and the metallic electrode surface (Figure S16). Once the pellets were prepared, they were carefully checked for any breakage or crack during making. It was also made sure that, no electrical conductance existed between the two opposite faces of the pellet that could create ambiguity in the proton conductivity measurement. Once the pellets were prepared, the diameter of the circular face and thickness of the pellet were measured carefully.

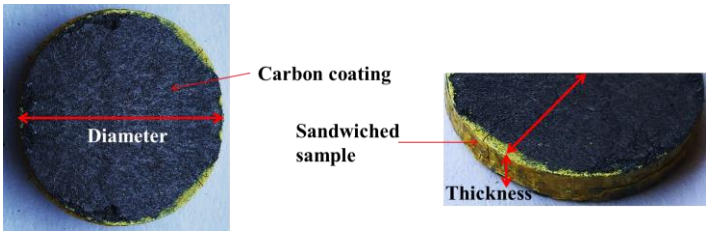

Figure S16. Top face of sample pellet (left) and side-view of pellet (right).

Cell set up and general experimental methodology:

All the impedance spectra were recorded at open circuit potential of each of the sample pellet. A sinusoidal signal of 5 mV was applied over a frequency range from 1 Hz to 10^6 Hz. The electrochemical workstation was attached with a stainless steel-made two-electrode set up kept inside an incubator. Graphical representations along with the respective images of the two electrode home-made cell are provided from Figure S17 to Figure S19. The complete detail of the two electrode cell is provided below.

The complete structure of the metallic stainless steel made circuit present inside the incubator/BOD box

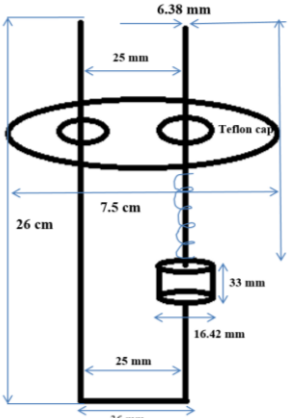

Figure S17. Image of the compelete two electrode set up used (in the left) and its schematic diagram (in the right)

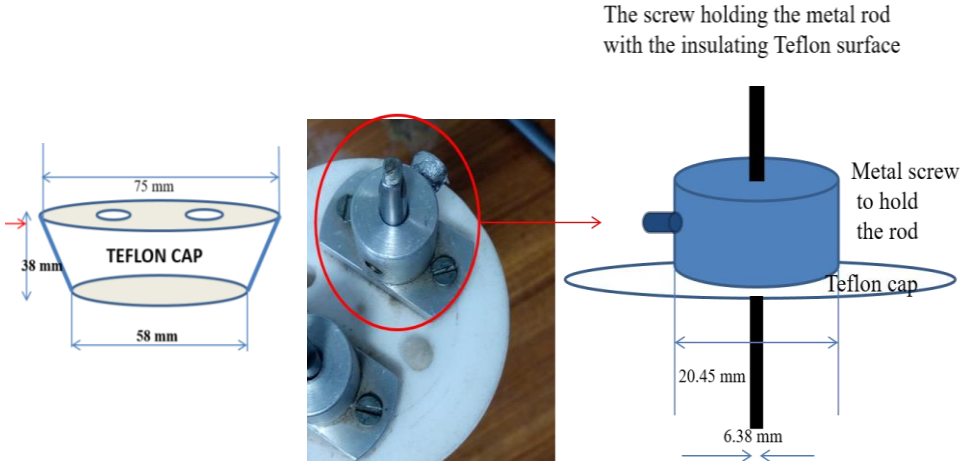

Figure S18. Schemtic representation of the top teflon cap holding the two electrodes (in the left) and image (in the middle) and schematic represenation (in the right) of the junction where electrical connections were made.

Using the two electrode set up kept inside incubator impedance measurements were carried out between a temperature range from 10 °C to 50 °C and relative humidity between 30% - 98%. The incubator was not efficient enough to hold the relative humidity ≥95% at high temperature measurement condition. Thus, we used a home-made set up (Figure S19). The set-up consists of (1) a conical flask of 5 L, (2) a heating source to heat water (3) 1-2 L of distilled water inside the conical flask (4) the two electrode set up described before fitted with a digital thermometer to check the temperature. The length of the metallic thermometer was adjusted such that, it could measure temperature near to the pellet. The Teflon lid holding the two-electrode set up, and digital thermometer was fitted on the top of the flask containing water with stand and clamp and sealed with Teflon tape. A small pinhole was kept on the Teflon lid to releases excess pressure developed inside the flask as a result of water vapor generation. The whole set up was heated thereafter to maintain the temperature and also to generate sufficient humidity. The water vapors maintain the near saturated relative humidity (≥95%) as well as the temperature inside the system. The set up (Figure S19) was held at a constant temperature for a period of 4 hours before recording each conductivity data so that equilibrium can be attained.

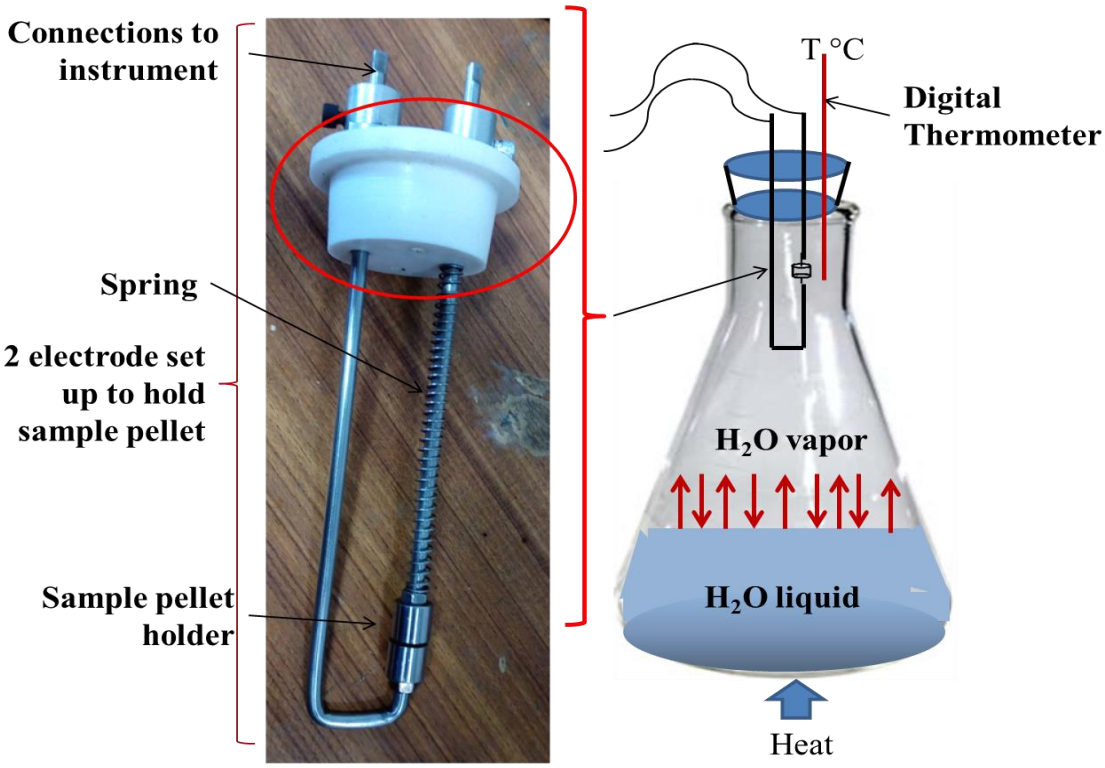

Figure 19. Graphical representation of the home-made set up for proton conductivity measurement at relative humidity ≥ 95 % and temperature ≥ 50 °C.

(b) Proton conductivity measurement under various temperature:

Proton conductivity was measured *via* impedance spectroscopic analysis of the samples. Impedance spectra of **PSM 1** and **PSM 2** were recorded at various temperatures and ≥ 95% relative humidity unless mentioned otherwise. Impedance spectra of **PSM 1** (Figure S20 to Figure S22) and **PSM 2** (Figure S23 and Figure S24) at various temperatures are given below. For each sample, impedance spectra were recorded during heating as well as cooling. Spectra of heating and cooling did not superpose with each other at any individual temperature. This is expected due to the differential water content in the channel of UiO-66

framework during heating and cooling cycle. While cooling, the sample pellet does not lose the adsorbed water molecule easily and show different impedance spectra than during heating cycle. For all the calculations impedance spectra recorded during heating cycle was analyzed and not the one recorded during cooling cycle.

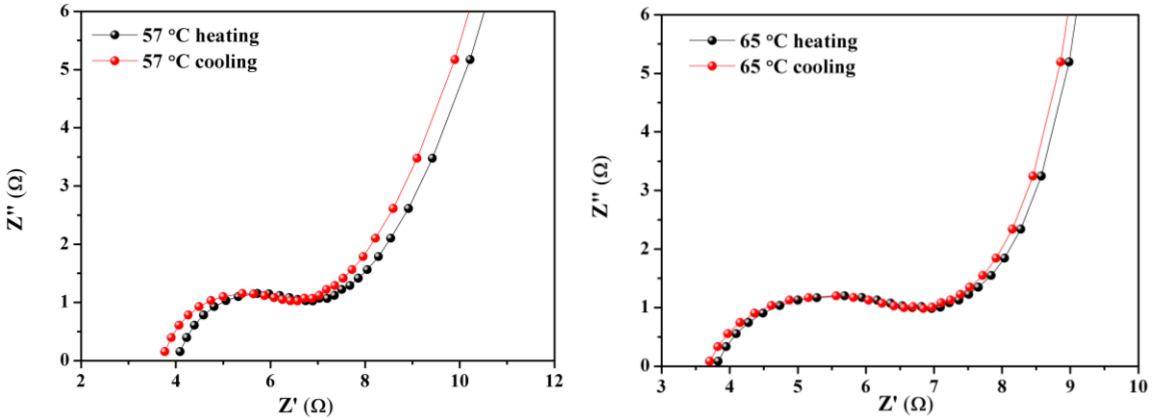

Figure S20. Nyquist plot of impedance spectra recorded during heating and cooling cycles. Left: **PSM 1** at 57 °C. Right: **PSM 1** at 65 °C.

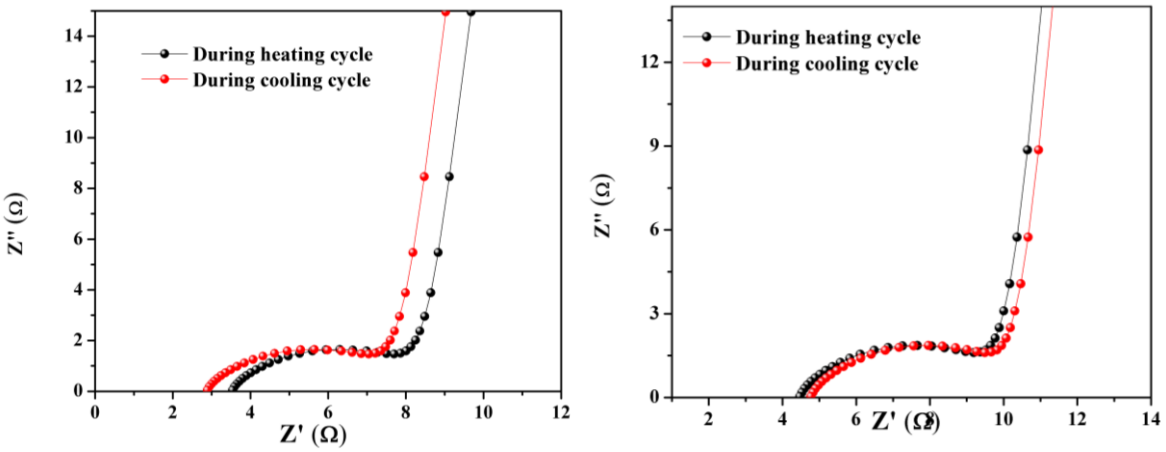

Figure S21. Nyquist plot of impedance spectra of **PSM 1** at 46.5 °C (at left) and at 31.8 °C (at right) of heating as well as cooling cycle.

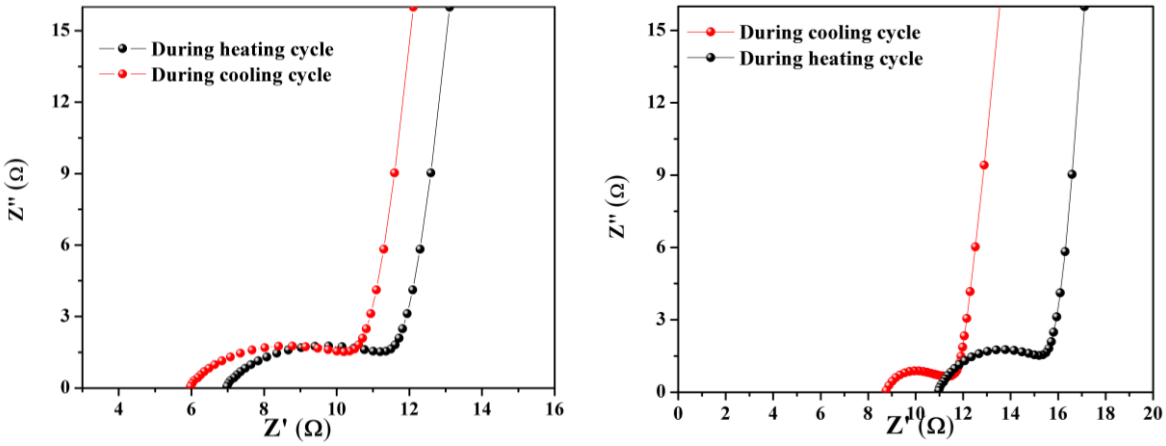

Figure S22. Nyquist plot of impedance spectra of **PSM 1** at 23. °C (at left) and at 11.6 °C (at right) of heating as well as cooling cycle.

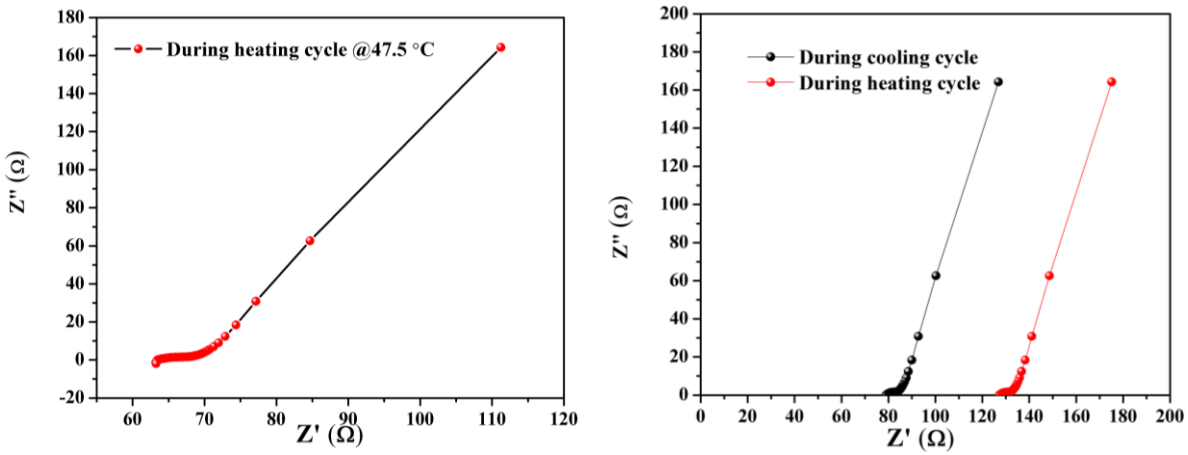

Figure S23. Nyquist plot of impedance spectra of **PSM 2** at 47.5 °C (at left) and at 39.2 °C (at right). Impedance spectra was recorded at 47.5 °C only during heating cycle, while at 39.2 °C it was recorded during heating as well as cooling cycle.

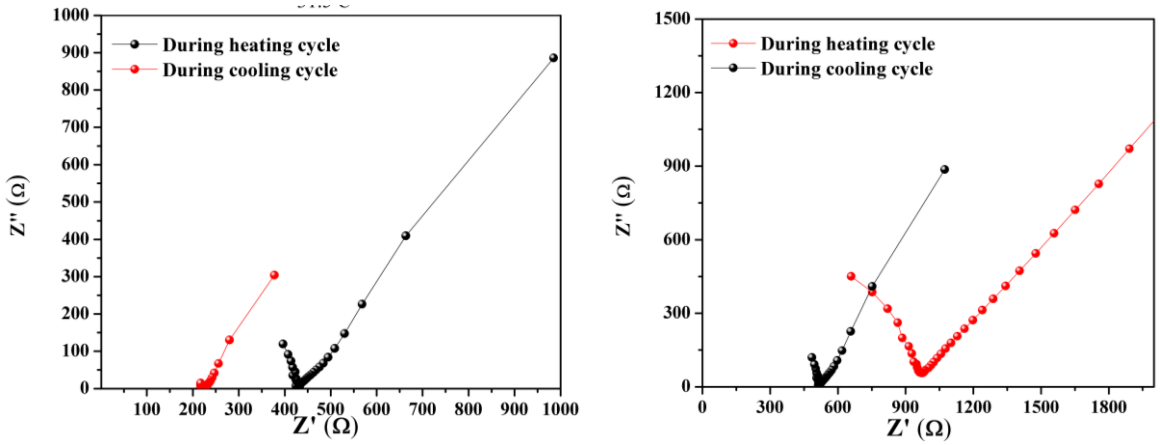

Figure S24. Nyquist plot of impedance spectra of **PSM 2** at 31.5 °C (at left) and at 24.2 °C (at right) of heating as well as cooling cycle.

(c) Proton conductivity measurement under different relative humidity:

To understand the effect of humidity on the proton conductivity of **PSM 1** and **PSM 2**, impedance spectra were also recorded at 30 °C under various relative humidity for each sample. As expected from the water absorptivity of both **PSM 1** and **PSM 2** (*vide supra*) proton conductivity was found to increase rapidly at the moderate humidity region (relative humidity 30%-70% region). In the high humidity region (RH ≥ 70%) proton conductivity trend becomes relatively stable *i.e.*, it increases with a gradual small increment as the humidity is increased (Figure S25). As we have seen from water sorption isotherm of **PSM 1** and **PSM 2**, the adsorptivity increases rapidly in the moderate P/P_0 region while the rate of

increment of water sorption decreases when saturation approaches ($P/P_0 \approx 1$). Following a similar trend in impedance spectra of **PSM 1** and **PSM 2**, has significant implications because it provides a hint towards the mechanism of proton conduction to follow water assisted Grotthus mechanism in all these measurements.

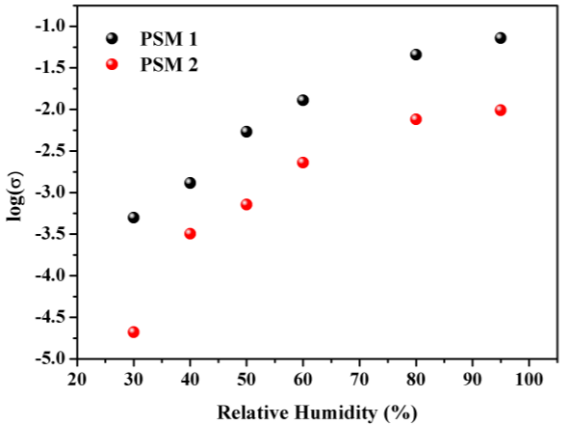

. **Figure S25.** Plot of log(conductivity) *vs.* relative humidity of **PSM 1** and **PSM 2** at 30 °C.

(d) Conductivity of PSM 1-Li:

Proton conductivity of **PSM 1**-Li was measured to understand if there is any role of any mobile charge carrier other than proton in the observed conductivity of the post synthetically modified compounds i.e., **PSM 1** and **PSM 2**. According to our expectation, **PSM 1**-Li showed conductivity in the order of 10^{-5} Scm^{-1}, which is pretty low compared to **PSM 1** or **PSM 2** and lies in the range of previously reported proton conductivity of pristine UiO-66-NH_2. This confirms the fact that, once the labile protons are substituted by lithium in **PSM 1**-Li, the conductivity falls rapidly due to lacking of mobile charge carrier. Thus, we could arrive at the conclusion that, the conductivity shown by either of the post synthetically modified compound was due to their labile protons and no contribution from any other labile charge carrier was needed to be taken into account. Impedance spectrum of **PSM 1**-Li is provided below (Figure S26)

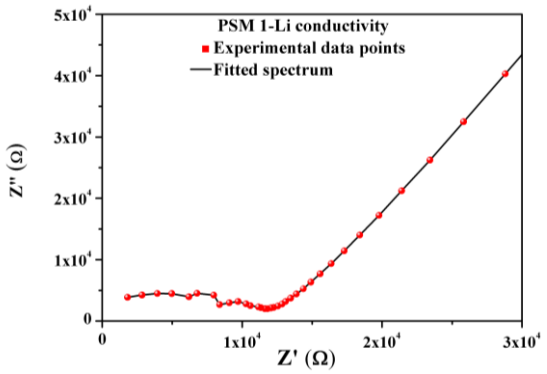

Figure S26. Nyquist plot of impedance spectra of **PSM 1**-Li showing conductivity in the range of 10^{-5} Scm^{-1}at 30 °C temperature and 95 % relative humidity.

Calculation of proton conductivity from Impedance spectra by fitting with equivalent circuit:

Equivalent circuit:

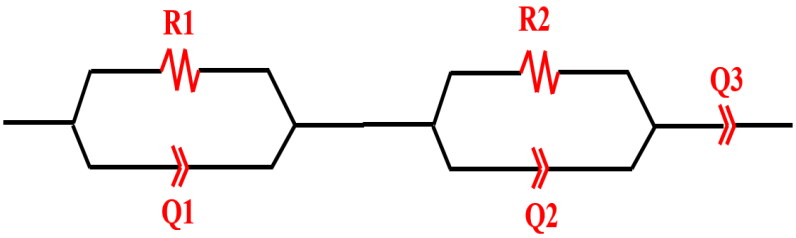

Impedance data were fitted to the most suitable equivalent circuit mentioned above with the help of EC-Lab software. The equivalent circuit is composed of three major components connected to each other in series. The pellet impedance (Z1), impedance at the electrode electrolyte junction/interface (Z2) and a constant phase element (Q3) are connected in series. The constant phase element (Q3) accounts for the linear low frequency region of the Nyquist plot of impedance spectrum. Z1 is composed of a resistance (R1) and constant phase element (Q1) connected to each other in parallel mode. Similarly Z2 consists of a resistance (R2) and a constant phase element (Q2) connected in parallel mode. Here R1 accounts for the bulk resistance of the pellet while R2 represents the charge transfer resistance existing between the electrodes and the pellet electrolyte. Here, it should be noted that, charge transfer resistance R2 is not associated with the conductivity of the electrolyte. Instead R1 is the crucial factor which quantifies the resistance of the bulk electrolyte. R2 depends mainly on the particle size, is a combination of (a) resistance created between the carbon paper and sample particles (b) inter-grain resistance (c) resistance existing between electrode surface and carbon paper of pellet. Use of (a) different coating method (e.g., use of silver paint instead of carbon paper) (b) different methods to prepare pellet with more intimate contact between the particles (c) use of thin film instead of pellet can be useful to reduce the value of R2 in actual application. On the other hand, the bulk resistance of electrolyte i.e., R1 is of our primary interest as it represents conductivity of the bulk pellet, which in this case is the proton conductivity of the pellet. R1 depends on (a) intrinsic conductivity of the pelletized sample (b) thickness of the pellet and (c) area of cross section of the pellet. Thus, to determine the proton conductivity of the pelletized sample from the R1 value both of the other two factors (i.e., area of cross section and thickness of pellet) should be taken as unity.

Here we provide the values of R1, and R2 by fitting the experimentally obtained data points along the curve generated by the equivalent circuit mentioned above. The accuracy of the fitting was measured by the factor χ^2.

Table S3. Table of fitting parameters to determine proton conductivity of PSM 1 in various temperatures:

Temp. (°C)	Software used	Value of R1(Ω)	Conductivity (Scm^{-1})	χ^2 value
80	EC-Lab V10.21	1.148	$\mathbf{1.63\times10^{-1}}$	7.76×10^{-3}
65	EC-Lab V10.21	1.225	$\mathbf{1.01\times10^{-1}}$	7.82×10^{-3}
48.5	EC-Lab V10.21	1.462	$\mathbf{8.51\times10^{-2}}$	2.9×10^{-3}
40.5	EC-Lab V10.21	1.559	$\mathbf{7.98\times10^{-2}}$	9.078×10^{-3}
35.8	EC-Lab V10.21	1.622	$\mathbf{7.67\times10^{-2}}$	5.114×10^{-3}
29.8	EC-Lab V10.21	1.74	$\mathbf{7.15\times10^{-2}}$	4.413×10^{-3}
23.2	EC-Lab V10.21	1.82	$\mathbf{6.83\times10^{-2}}$	1.303×10^{-3}
11.5	EC-Lab V10.21	2.13	$\mathbf{5.83\times10^{-2}}$	0.818×10^{-3}
9.7	EC-Lab V10.21	2.18	$\mathbf{5.70\times10^{-2}}$	0.384×10^{-3}

Table S4. Table of fitting parameters to determine proton conductivity of PSM 2 in various temperatures:

Temp. (°C)	Software	Value of R1(Ω)	Conductivity (Scm^{-1})	χ^2 value
80	EC-Lab V10.21	26.98	$\mathbf{4.6\times10^{-3}}$	9.14×10^{-3}
70	EC-Lab V10.21	33.55	$\mathbf{3.7\times10^{-3}}$	1.13×10^{-2}
47.5	EC-Lab V10.21	63.46	$\mathbf{1.95\times10^{-3}}$	3.57×10^{-3}
39	EC-Lab V10.21	79.68	$\mathbf{1.56\times10^{-3}}$	2.9×10^{-3}
31.5	EC-Lab V10.21	100	$\mathbf{1.24\times10^{-3}}$	0.8×10^{-3}
16.9	EC-Lab V10.21	183	$\mathbf{0.68\times10^{-3}}$	2.68×10^{-3}
10.1	EC-Lab V10.21	209	$\mathbf{0.59\times10^{-3}}$	0.22×10^{-3}

Calculation of proton conductivity from the R1 value for PSM 1 at 80 °C (all other proton conductivity values were calculated using similar method:

Value of R1 =1.148 Ω.

Now we know, Conductance **(L) = (1/R) = σ × (A/d)** ……. Eqn (1)

Thus, conductivity (**σ**) = (L) × **d/A** = (1/**R**) × (**d/A**) …….. Eqn (2)

Where R is resistance of sample; **σ** is conductivity of the sample;

d = thickness of pellet = 0.25 cm for **PSM 1** for the high temperature measurements while d = 0.165 cm for **PSM 1** low temperature measurements (≤50 °C). Two different pellets were used for the two measurements.

A = area of cross section of pellet = 1.32665 cm^2.

Putting the value R1 =1.148 Ω, in Eqn (2) we get the conductivity of **PSM 1** at 80 °C.

Conductivity of **PSM 1** at 80 °C is $(\sigma)_{80\,^{\circ}C} = \mathbf{1.64 \times 10^{-1}}$ Scm^{-1}.

All the conductivity data for **PSM 1** and **PSM 2** were calculated using similar data fitting and similar calculations.

Section S14: Stability check and reusability check of PSM 1 and PSM 2

Stability of **PSM 1** was verified by proton conductivity measurement of **PSM 1** at 80 °C under relative humidity of 95% over a period of 48 hours. Each conductivity measurements were carried out at an interval of 12 hours. The proton conductivity data shows no significant change in the conductivity values (Figure 29 (right)). Thus, the long term stability of **PSM 1** was verified under operational condition.

Reusability of **PSM 1** and **PSM 2** were checked by measuring proton conductivity *via* impedance spectroscopy for 5 consecutive heating and cooling cycles. Proton conductivity values were found to be highly reproducible for both the compounds. From Figure S27 (left) it can be seen that **PSM 1** functions as efficient proton conductor for cycles of measurement.

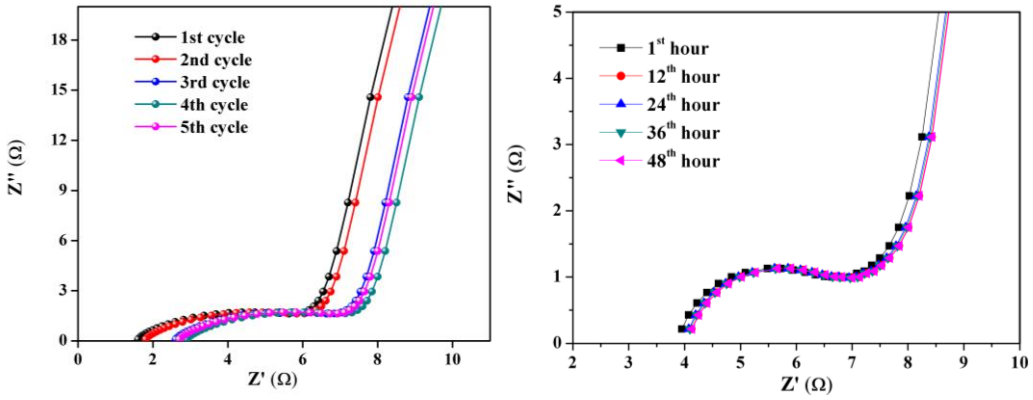

Figure S27. Nyquist plot of impedance spectra of **PSM 1**. Impedance spectra were recorded for consecutive 5 heating cycles (10 °C to 50 °C) using same pellet of **PSM 1** (left). Measurement was also done at 80 °C for 48 hours (right).

Apart from measuring proton conductivity of the samples (*i.e.*, **PSM 1** and **PSM 2**) PXRD and FT-IR analysis were also performed to check the robustness of the material as proton conducting material. After each heating cycle, **PSM 1** and **PSM 2** were examined by powdered XRD and FT-IR measurement. Both the compounds **PSM 1** and **PSM 2** were found to be stable towards multiple cycle of operation. The result can be confirmed from the Figure S28, Figure S29 and Figure S30.

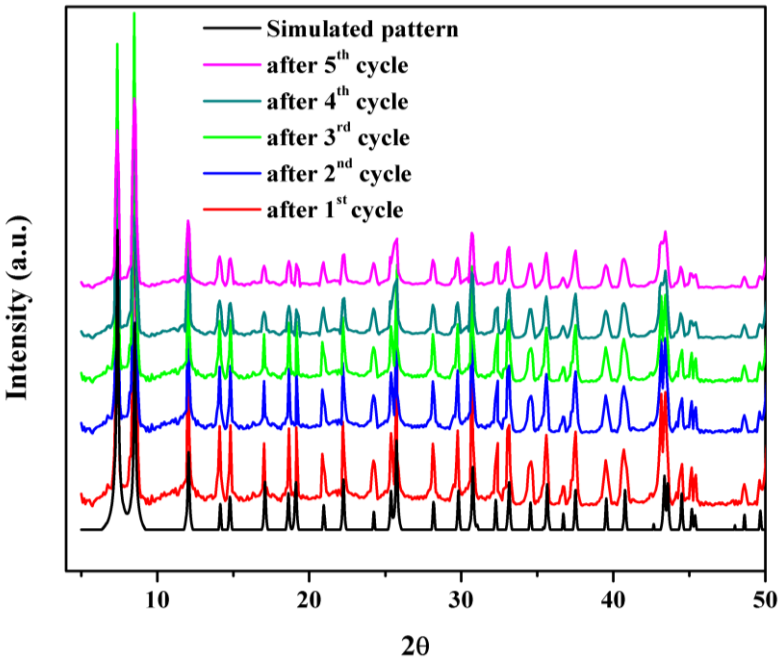

Figure S28. PXRD patterns of **PSM 1** after 5 consecutive heating cycles (temperature from 8 °C to 50 °C) and impedance measurement, compared with the simulated PXRD pattern of UiO-66.

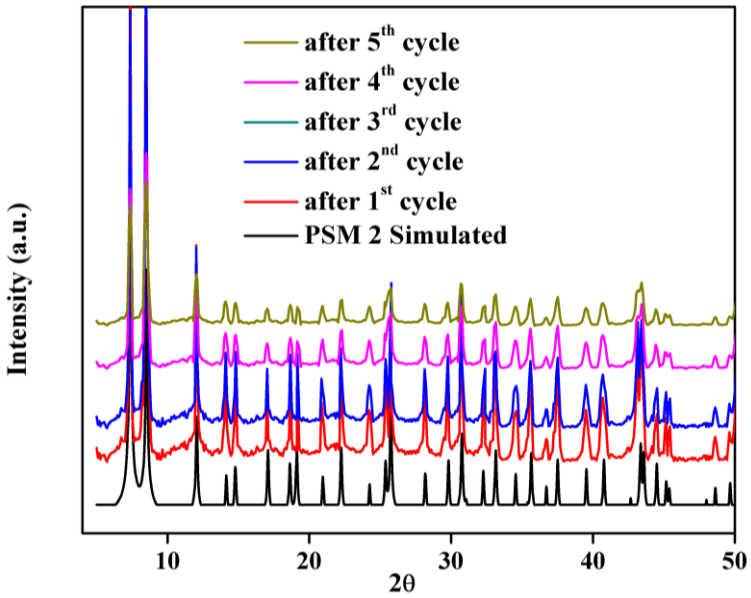

Figure S29. PXRD patterns of **PSM 2** after 5 consecutive heating cycles (temperature from 8 °C to 50 °C) and impedance measurement, compared with the simulated PXRD pattern of UiO-66.

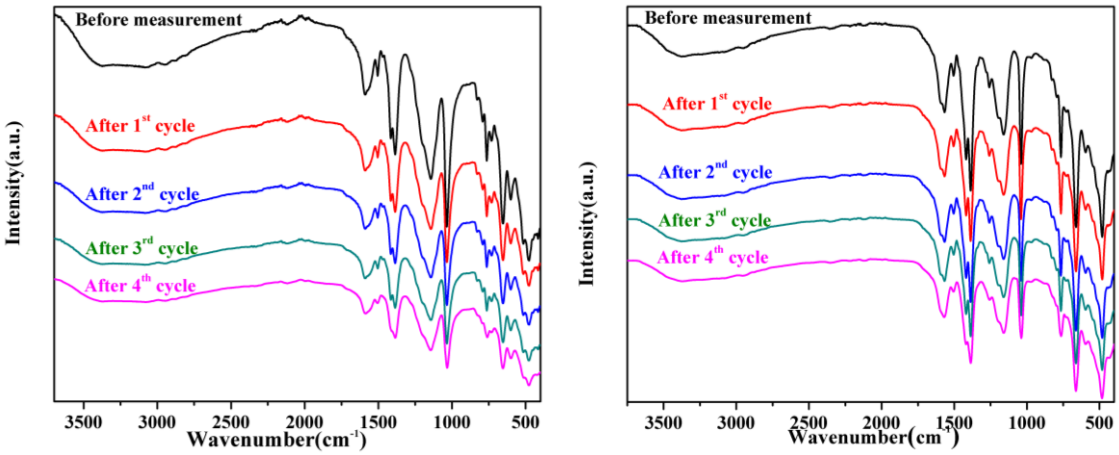

Figure S30. FT-IR spectra of **PSM 1** (left one) and **PSM 2** (right one) after 5 consecutive heating cycles (temperature from 8 °C to 50 °C) and impedance measurement.

Besides, N_2 sorption analysis (Figure S31) was carried out on **PSM 1** after 5 cycles of proton conductivity measurement to understand if long term usage is causing any change in the microstructure of the parent MOF structure. BET surface area of 310.5 m^2/g was observed for **PSM 1** after 5 cycles of proton conductivity measurement. This negligible change in the BET surface area before and after proton conductivity studies confirm that no significant change *i.e.*, destruction of porous framework structure is occurring in the sample. This observation again strengthens our claim of **PSM 1** to be a robust and efficient proton conductor.

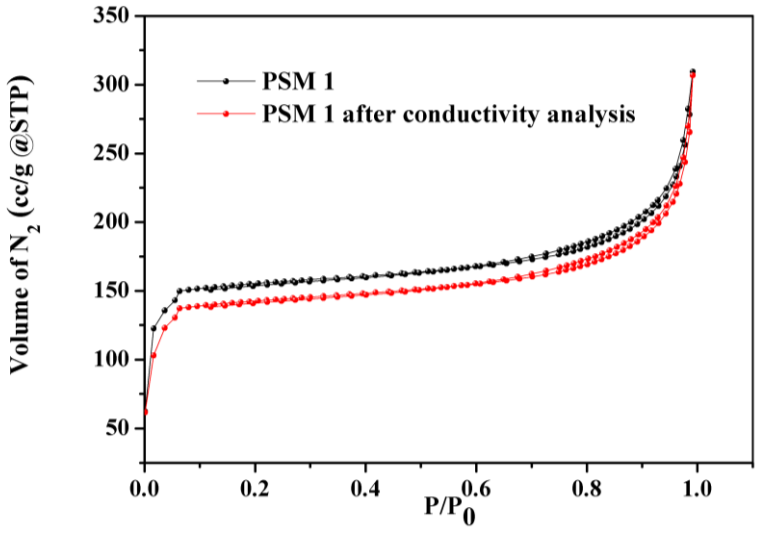

Figure S31. N_2 sorption isotherm of **PSM 1** after 4 cycles of proton conductivity measurements.

Section S15. Activation energy calculation:

Activation energy (E_a) of proton conductivity was calculated for **PSM 1** and **PSM 2** from their proton conductivity values at various temperatures. Derived plot was constructed

between **ln(σT)** and **1000/T** for **PSM 1** as well as **PSM 2** (refer to main manuscript). Activation energy of proton conductivity was calculated from the slope of the plot with the help of Arrhenius equation. Detailed calculation is given below.

Calculation of activation energy:

From Arrhenius Equation, $\boldsymbol{\sigma T = \sigma_0 \times \exp(-E_a/RT)}$ …… Eqn. (3)

Where, **σ** = conductivity of the sample, i.e., here proton conductivity; $\mathbf{E_a}$ = Activation energy of proton conduction; R= Ideal gas constant; T= Temperature in Kelvin scale.

Eqn. (3) can be restructured as $\boldsymbol{\ln(\sigma T) = \ln\sigma_0 - (Ea/RT)}$

It can be written as $\boldsymbol{\ln(\sigma T) = \ln\sigma_0 + (-E_a/(1000\times R))(1000/T)}$ … Eqn. (4)

Eqn. (4) also represents the straight line plot obtained between **ln(σT)** and. **1000/T**

Thus, Slope (**m**) = $\boldsymbol{(-E_a/1000\times R)}$ = 1.24168 $Scm^{-1}K^2$.

Activation energy of **PSM 1** $\boldsymbol{(E_a)_{PSM\ 1}}$ **= 0.107 eV**.

On the other hand activation energy of **PSM 2** $\boldsymbol{(E_a)_{PSM\ 2}}$ **= 0.292 eV**.

Section S16. Computational details and the ground energy minimized structures of the model systems:

Restricted density functional theory (DFT) was applied to calculate the closed-shell ground energy minimized structures of the model pendant of **PSM 1**, **PSM 2** and UiO-66-NH_2 and their respective anionic counter parts. The B3LYP functional and 6-31G** basis set was used throughout the present study. The energy minimum structure was confirmed by performing subsequent Hessian calculations at the respective optimized geometry. The optimized structures and the corresponding xyz coordinates of the model systems are given in Table SX. All calculations were performed with methods implemented in the Gaussian-09 programs module.

Table S5. The energy minimum structure at the ground electronic state of model PSM 1 in water and its xyz coordinates:

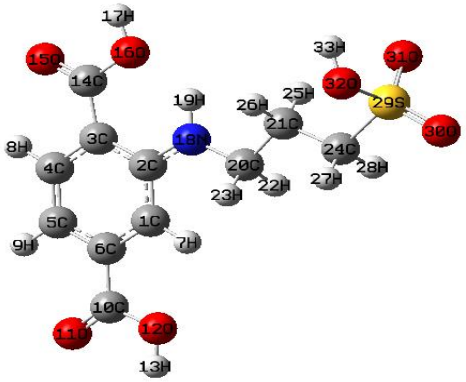

C	-2.113708322914	-0.872609148099	0.004331668588
C	-1.566744157859	0.436525853077	0.013690051640
C	-2.489523985605	1.534043042725	0.011415246195
C	-3.872933182208	1.274374222828	0.007625001189
C	-4.385769464149	-0.008783061795	0.003775338926
C	-3.486975779011	-1.088376694744	0.001328097072
H	-1.451614237370	-1.726861006699	0.000448937713
H	-4.536561157832	2.131400952348	0.006075098371
H	-5.452525578783	-0.194030124077	0.000660535697
C	-4.052800333555	-2.469061690176	-0.005614711312
O	-5.244827390452	-2.720691331255	-0.008993974421
O	-3.110651675027	-3.434868189557	-0.007170245142
H	-3.576155078650	-4.288839789032	-0.011480310738
C	-2.124827643805	2.969664721341	0.007263696779
O	-2.925557726967	3.890510275448	0.008063257793
O	-0.788070264416	3.216479597328	0.000002457323
H	-0.673514091302	4.182311090745	-0.007090441785
N	-0.213442315947	0.599805654561	0.033156692556
H	0.135597764506	1.545025486456	-0.023643855935
C	0.746297830823	-0.488334535205	-0.046191334589
C	2.168523323417	0.078979337948	-0.001481724144
H	0.605290171650	-1.065547407103	-0.971705799161
H	0.602556568864	-1.184179153679	0.791254020058
C	3.200810096742	-1.039513263423	-0.124094397389
H	2.306270421555	0.791941326007	-0.820717907776
H	2.315414264940	0.617708730672	0.940110762318
H	3.140715015997	-1.761848628101	0.694037002574
H	3.111222418174	-1.581171151045	-1.070432319881
S	4.903154316791	-0.444040596677	-0.113757281415
O	5.799756124372	-1.595371146484	-0.189018729462
O	5.060844542490	0.673927044410	-1.049362217593
O	5.033561004989	0.151067295163	1.405762070364
H	5.112662520544	1.120417286093	1.351384315586

Table S6. The energy minimum structure at the ground electronic state of model PSM 1 anion in water and its xyz coordinates:

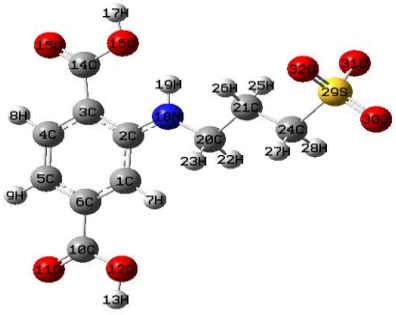

C	-2.09385100	-0.87588900	-0.00598900
C	-1.54650600	0.43462300	-0.00421400
C	-2.47187100	1.53129000	0.00267400
C	-3.85522900	1.26955200	0.01079200
C	-4.36695300	-0.01374100	0.01177000
C	-3.46635600	-1.09271300	0.00299600
H	-1.42955700	-1.72835500	-0.01395200
H	-4.51973400	2.12595800	0.01597400
H	-5.43347700	-0.20019300	0.01839900
C	-4.03088000	-2.47372100	0.00375400
O	-5.22274000	-2.72696000	0.00991400
O	-3.08828500	-3.43932900	-0.00242000
H	-3.55397400	-4.29317600	-0.00092600
C	-2.10948000	2.96657000	0.00048700
O	-2.91120700	3.88720900	0.00696500
O	-0.77300700	3.21607500	-0.01046900
H	-0.66142000	4.18223100	-0.01244600
N	-0.19562700	0.59617700	-0.00556400
H	0.15626200	1.54157900	-0.02450000
C	0.77320000	-0.48968900	-0.03801800
C	2.19273400	0.08003000	-0.00973200
H	0.63396800	-1.10077100	-0.94175100
H	0.62518800	-1.15627100	0.82325600
C	3.25395900	-1.01535300	-0.05991100
H	2.33422900	0.75485300	-0.86133100
H	2.33056300	0.67155200	0.90200000
H	3.15592400	-1.70609300	0.78328100
H	3.18413900	-1.59734300	-0.98396900
S	4.94965300	-0.36049600	0.01093700
O	5.82507000	-1.56863000	-0.05932700
O	5.08475800	0.53888700	-1.17499900
O	5.04543800	0.36462100	1.31437100

Table S7. The energy minimum structure at the ground electronic state of model PSM 2 in water and its xyz coordinates:

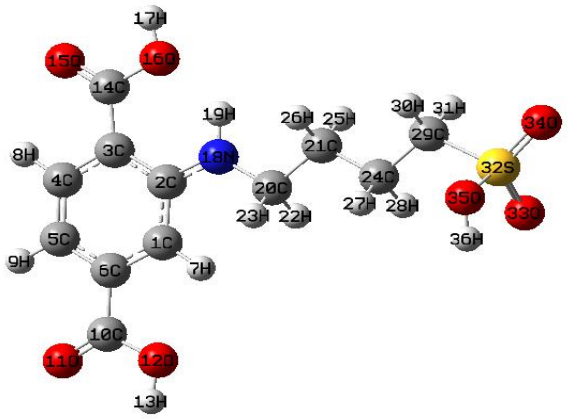

C	-2.445477799037	0.906134633381	0.007323723810
C	-2.152825877251	-0.483158433791	-0.005160041650
C	-3.266123076095	-1.387689097195	-0.016542744731
C	-4.576297421105	-0.872584661703	-0.013561773080
C	-4.839633572222	0.483772232929	-0.000264706081
C	-3.753536503484	1.375461501912	0.010147061123
H	-1.634079323682	1.620111605630	0.014718956343
H	-5.388754562071	-1.590097283721	-0.022209762209
H	-5.852813833996	0.865760682017	0.002084928403
C	-4.048480831710	2.837913270691	0.024329413698
O	-5.171160397429	3.311214584951	0.025993134324
O	-2.940716055902	3.608456714974	0.035727339496
H	-3.237292865695	4.534620410400	0.044543610556
C	-3.177823783001	-2.865558898080	-0.031730945155
O	-4.137344749712	-3.619991904260	-0.040271567882
O	-1.911383899421	-3.359864370148	-0.036169679382
H	-1.981807800884	-4.329850372779	-0.046348936947
N	-0.855052633162	-0.894296913669	-0.005095366211
H	-0.685153823516	-1.888852636865	-0.018523390552
C	0.294610331891	-0.003558344911	0.004994186990
C	1.590580425415	-0.816540630607	0.018898971330
H	0.262913902276	0.650494374836	0.887882335921
H	0.279805354949	0.651028521142	-0.878268873317
C	2.828996148541	0.089167357504	0.021604692968
H	1.601508180646	-1.462433293577	0.905525920125

H	1.614327263422	-1.474234002727	-0.858784562237
H	2.828764998279	0.719245337134	-0.874213291098
H	2.804409642472	0.754904368437	0.890344194428
C	4.112089974785	-0.740067420122	0.059751987987
H	4.219753640632	-1.390350054465	-0.812394654922
H	4.175348351337	-1.358763566367	0.960029412525
S	5.616080581229	0.254662220918	0.102485627882
O	5.508352019417	1.308267740428	1.117427094169
O	6.772011401512	-0.640426259642	0.098314745739
O	5.578264778060	0.973539434583	-1.368928697333
H	5.425150814510	1.926756152759	-1.240538345028

Table S8. The energy minimum structure at the ground electronic state of model PSM 2 anion in water and its xyz coordinates:

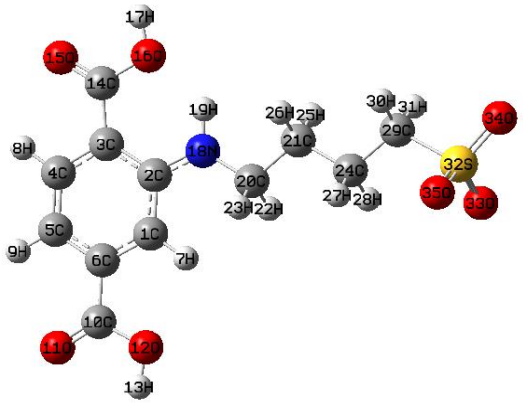

C	-2.42726600	-0.90603700	-0.00855600
C	-2.12943500	0.48284600	-0.01001500
C	-3.24038300	1.39085300	0.00370400
C	-4.55226600	0.87964000	0.01553400
C	-4.82007400	-0.47573900	0.01501000
C	-3.73652100	-1.37103200	0.00281200
H	-1.61774100	-1.62207500	-0.01687400
H	-5.36235000	1.59985500	0.02564600
H	-5.83439500	-0.85459900	0.02402800
C	-4.03615100	-2.83252000	0.00237100
O	-5.16026800	-3.30243200	0.01592900
O	-2.93112800	-3.60693100	-0.01543200
H	-3.23099300	-4.53206000	-0.01438700
C	-3.14769700	2.86812100	0.00837100

O	-4.10486200	3.62588800	0.02042100
O	-1.87987300	3.35905300	-0.00134600
H	-1.94822400	4.32920000	0.00419700
N	-0.83090800	0.88820000	-0.02648900
H	-0.65633900	1.88186700	-0.01225600
C	0.31834400	-0.00518800	-0.01836300
C	1.61866600	0.79987200	-0.04766000
H	0.28343300	-0.67643800	-0.88812700
H	0.29959300	-0.64325400	0.87716100
C	2.85792000	-0.10237100	-0.01611800
H	1.63452800	1.42336800	-0.95099400
H	1.63777300	1.48373200	0.81095400
H	2.85250300	-0.70770700	0.89765500
H	2.83321700	-0.80051200	-0.86054300
C	4.15862100	0.69589600	-0.07338200
H	4.22747800	1.40399500	0.75857700
H	4.23435700	1.26449200	-1.00557800
S	5.65010200	-0.33932200	0.01671500
O	5.56216900	-1.28171700	-1.14082900
O	6.78729100	0.62416600	-0.09274200
O	5.58658800	-1.02854700	1.34228400

Table S9. The energy minimum structure at the ground electronic state of model UiO-66-NH_2 in water and its xyz coordinates:

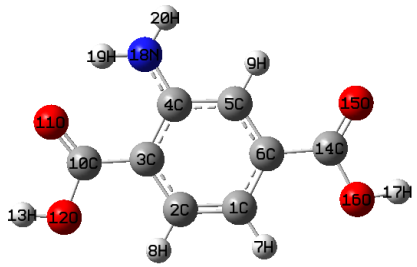

C	0.884564567946	-1.355412320718	-0.006301112104
C	-0.497754027105	-1.397595425940	-0.010802798871
C	-1.279566397731	-0.224777901423	-0.017134355821
C	-0.635877087902	1.050455857689	-0.026386671467
C	0.778156076541	1.073516205659	-0.014208332257
C	1.521123455917	-0.098344790361	-0.004959243159
H	1.467876255842	-2.266932074394	-0.000575216843
H	-1.006530332353	-2.353923005277	-0.005062974663
H	1.297173690695	2.026170116154	-0.015448270450

C	-2.749444860035	-0.315730004976	0.004393037902
O	-3.523364533482	0.638421157624	0.032515670553
O	-3.216478801772	-1.583566349960	-0.005034429677
H	-4.186654709870	-1.523547135176	0.016840937036
C	3.008078758496	0.031171403367	0.006309992966
O	3.610886769626	1.089925219614	0.011077228091
O	3.639499314820	-1.160654576583	0.010443345439
H	4.594968595663	-0.978667209291	0.017245555491
N	-1.328563910275	2.220811142505	-0.079014061030
H	-2.329161482844	2.181034990379	0.061077452350
H	-0.842238342179	3.084158701108	0.105260246514

Table S10. The energy minimum structure at the ground electronic state of model UiO-66-NH_2 anion in water and its xyz coordinates:

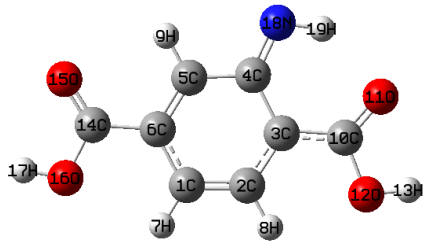

C	0.843676585031	-1.336621176141	-0.000087715630
C	-0.531973879034	-1.343468789018	-0.000108093148
C	-1.314949486496	-0.158746944433	-0.000149497168
C	-0.660780060223	1.159526940834	-0.000146806819
C	0.792593186264	1.100989998205	-0.000124006737
C	1.509819550804	-0.071644755505	-0.000100875942
H	1.411374015804	-2.258203954061	-0.000067344660
H	-1.054169528208	-2.294890230930	-0.000102904397
H	1.318058787135	2.050604201677	-0.000129239303
C	-2.756396021624	-0.256370015477	-0.000184572188
O	-3.570050501430	0.677795023405	-0.000085859203
O	-3.245247689006	-1.543348939638	0.000047701584
H	-4.210714240929	-1.441072145891	0.000120212858
C	2.993135137979	0.027241211490	-0.000087421109
O	3.640034284070	1.063441107903	0.000156301466
O	3.607607164147	-1.181957704107	0.000021527326
H	4.563552520338	-1.004413843739	0.000175877326
N	-1.221905416780	2.352327837908	-0.000237332380
H	-2.234324407843	2.215038177518	-0.000288951876

Section S17. Determination of acid dissociation constant (pK_a) of the model PSM 1, PSM 2 and UiO-66-NH_2:

The pK_a value of the model **PSM 1**, **PSM 2** and UiO-66-NH_2 were calculated by using text book thermodynamic cycle and thermodynamic formulation. The thermodynamic cycle is presented in scheme 1, where AH represents the undissociated form of the model system and A^- is the anion after removal of a proton (H^+) from the model system. The well-known thermodynamic formulation of pK_a is given as follows:

$$\Delta G^0_{aq} = -2.303RT \log K_a \quad (1)$$

$$pK_a = \Delta G^0_{aq}/2.303RT \quad (2)$$

Where, ΔG^0_{aq} represents the overall change of standard free energy in aqueous medium and R and T possess their usual meaning. The temperature considered here is the room temperature, 298.15 K. The $\Delta G^0_{aq,}$ associated with the dissociation in the aqueous medium can be calculated using thermodynamic cycle shown in Scheme S1. It should be mentioned that we have used the experimental formation free energy (-6.28 kcal/mol) and the hydration free energy change (-264.61 kcal/mol) for proton in our calculation. The conversion of the standard state of gas phase into the aqueous phase is performed by using following equation,

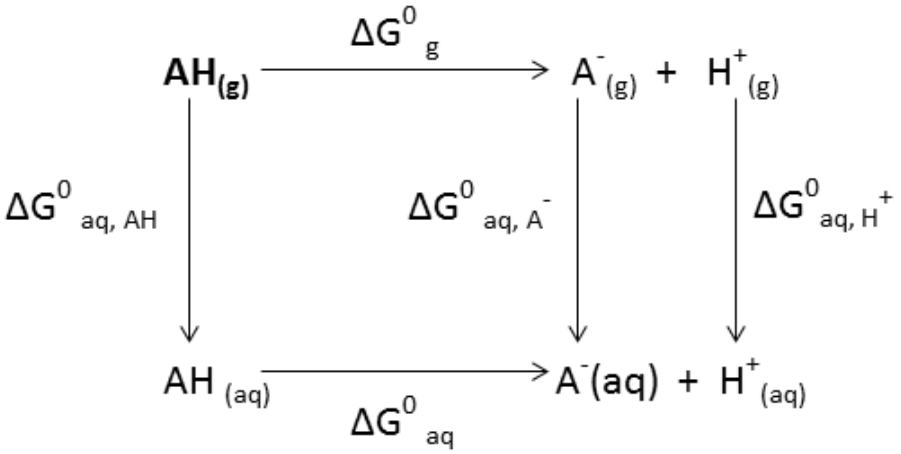

Scheme S1. Thermodynamic cycle for acid dissociation.

$$\Delta G^0_g\,(1\ mol/dm3) = \Delta G^0_g\,(1\ atm) + RT\ ln(24.46) \quad (3).$$

Following the above conversion equation the working equation for the ΔG^0_{aq} becomes

$$\Delta G^0_{aq} = [G^0_g\,(A^-) - G^0_g\,(AH) + \Delta G^0_{aq}\,(A^-) - \Delta G^0_{aq}\,(AH) - 269.0]\ kcal/mol \quad (4).$$

The calculated values of $G^0_g\,(A^-)$, $G^0_g\,(AH)$, $\Delta G^0_{aq}\,(A^-)$, $\Delta G^0_{aq}\,(AH)$, ΔG^0_{aq} and pK_a of the model **PSM 1**, **PSM 2** and UiO-66-NH_2 are given in Table S11.

Table S11. The estimated theoretical values of the pK_a and its parameters of the model PSM 1, PSM 2 and UiO-66-NH_2.

	G^0_g (A^-) Hartree	G^0_g (AH) Hartree	ΔG^0_{aq} (A^-) kcal/mol	ΔG^0_{aq} (AH) kcal/mol	ΔG^0_{aq} kcal/mol	pK_a
PSM 1	-1405.8043	-1406.3146	-62.12	-15.59	4.73	3.47
PSM 2	-1445.0908	-1445.6063	-64.12	-16.34	6.70	4.91
UiO-66-NH_2	-664.0902	-664.6675	-51.85	-7.68	49.10	35.99

Section S18. NBO analysis on model compounds of PSM 1 and PSM 2:

Table S12. Eletronic occupancy and energy of the nitrogen core 1s orbital of model compounds of PSM 1 and PSM 2.

PSM1: Natural Populations: Natural atomic orbital occupancies

NAO	Atom	No	lang	Type(AO)	Occupancy	Energy
206	N	18	S	Cor(1S)	1.99936	-14.18659 (eV)

Natural Bond Orbital Analysis:

(Occupancy) Bond orbital/ Coefficients/ Hybrids

50. (1.99936) CR (1) N 18 s(100.00%)p 0.00(0.00%)

1.0000 0.0001 0.0000 0.0000 0.0001

0.0000 0.0001 0.0000 -0.0002 0.0000

0.0000 0.0000 0.0000 0.0000 0.0000

PSM2

Natural Populations: Natural atomic orbital occupancies

NAO	Atom	No	lang	Type(AO)	Occupancy	Energy
206	N	18	S	Cor(1S)	1.99936	-14.18412 (eV)

Natural Bond Orbital analysis:

(Occupancy) Bond orbital/ Coefficients/ Hybrids

53. (1.99936) CR (1) N 18 s(100.00%)p 0.00(0.00%)

1.0000 0.0002 0.0000 0.0000 0.0001

0.0000 0.0002 0.0000 0.0000 0.0000

0.0000 0.0000 0.0000 0.0000 0.0000

Section S19. Tabular representation of various reported MOF based proton conductors and their conductivities:

Table S13. Reports of MOF based proton conductivity:

Sr. No.	MOF system	Proton Conductivity Value (Scm^{-1})	Temperature (°C) and Relative Humidity (%)	Activation energy (eV)	Reference No.
1.	[Cu(*p*-IPhHIDC)]$_n$	1.51×10^{-3}	100 °C and 98 % RH	0.25	3
2.	UiO-66-$(SO_3H)_2$	8.4×10^{-2}	80 °C, 90 % RH	0.32	4
3.	CPM-103 a	1.0×10^{-2}	22.5 °C, 75 % RH	0.66	5
4.	Fe-CAT-5	5.0×10^{-2}	25 °C, 98 % RH	0.24	6
5.	BUT-8(Cr)	4.63×10^{-2}	80 °C, 100 % RH	0.21	7
6.	BUT-8(Cr)A	$1.27 \text{ X } 10^{-1}$	80 °C, 100 %	0.11	7
7.	MSA-EIMS@MIL-101 MSA-EIMS	1.02×10^{-3}	150 °C	0.30	8
8.	FJU-17	1.08×10^{-2}	100 °C	0.29	9
9.	PCMOF2½(Triazole)	1.17×10^{-1}	85 °C, 90 %	0.22	10
10.	TfOH@MIL-101	8.0×10^{-2}	15 °C, 60 % RH	0.25	11
11.	VNU-15	2.9×10^{-2}	95 °C, 60 % RH	0.22	12
12.	MIL-101-SO_3H	1.16×10^{-2}	80 °C, 100 %	0.23	7
13.	PCMOF2½	2.1×10^{-2}	85 °C, 90 % RH	0.21	13
14.	PCMOF10	4.2×10^{-4}	70% and 70	0.4	14
15.	COG-10P	2.3×10^{-2}	60 °C	0.29	15
16.	UiO-66(Zr)-$(CO_2H)_2$	2.3×10^{-3}	90 °C, 95 % RH	0.17	16
17.	H_3PO_4@MIL-101	1.0×10^{-2}	140 °C, 1.10 % RH	0.25	17
18.	H_2SO_4@MIL-101 (2.7M)	1.0×10^{-2}	150 °C, 0.13 % RH	0.16	17
19.	PCMOF-5	2.5×10^{-3}	60 °C, 98 % RH	0.16	18
20.	MROF-1	1.72×10^{-2}	70 °C, 97 % RH	0.37	19
21.	**PSM 1**	**1.64×10^{-1}**	**80 °C, 95 % RH**	**0.107**	**Our Work**
22.	**PSM 2**	**4.6×10^{-3}**	**80 °C, 95 % RH**	**0.292**	**Our Work**

References:

1. Katz, M. J.; Brown, Z. J.; Colon, Y. J.; Siu, P. W. W.; Scheidt, K. A.; Snurr, R. Q.; Hupp, J. T.; Farha, O. K. A facile synthesis of UiO-66, UiO-67 and their derivatives. *Chem. Commun*. **2013**, *49*, 9449-9451.
2. Britt, D.; Lee, C.; Uribe-Romo, F. J.; Furukawa, H.; Yaghi, O. M. Ring-Opening Reactions within Porous Metal−Organic Frameworks. *Inorg. Chem*. **2010**, *49*, 6387-6389.
3. Sun, Z.; Yu, S.; Zhao, L.; Wang, J.; Li, Z.; Li, G. A Highly Stable Two-Dimensional Copper(II) Organic Framework for Proton Conduction and Ammonia Impedance Sensing. Chem. Eur. J. **2018**, *24*, 10829-10839.
4. Phang, W. J.; Jo, H.; Lee, W. R.; Song, J. H.; Yoo, K.; Kim, B.; Hong, C. S. Superprotonic Conductivity of a UiO-66 Framework Functionalized with Sulfonic Acid Groups by Facile Postsynthetic Oxidation. *Angew. Chem. Int. Ed*. **2015**, *54*, 5142-5146.
5. Zhai, Q. G.; Mao, C.; Zhao, X.; Lin, Q.; Bu, F.; Chen, X.; Bu, X.; Feng, P. Cooperative Crystallization of Heterometallic Indium–Chromium Metal–Organic Polyhedra and Their Fast Proton Conductivity. *Angew. Chem., Int. Ed*. **2015**, *54*, 7886-7890.
6. Nguyen, N. T. T.; Furukawa, H.; Gandara, F.; Trickett, C. A.; Jeong, H. M.; Cordova, K. E.; Yaghi, O. M. Three-Dimensional Metal-Catecholate Frameworks and Their Ultrahigh Proton Conductivity. *J. Am. Chem. Soc*. **2015**, *137*, 15394-15397.
7. Yang, F.; Xu, G.; Dou, Y.; Wang, B.; Zhang, H.; Wu, H.; Zhou, W.; Li, J. R.; Chen, B. A flexible metal–organic framework with a high density of sulfonic acid sites for proton conduction. *Nature Energy* **2017**, *2*, 877-883.
8. Chen, H.; Han, S. Y.; Liu, R. H.; Chen, T. F.; Bi, K. L.; Liang, J. B.; Deng, Y. H.; Wan, C. Q. High conductive, long-term durable, anhydrous proton conductive solid-state electrolyte based on a metal-organic framework impregnated with binary ionic liquids: Synthesis, characteristic and effect of anion. *J. Power Sources* **2018**, *376*, 168-176.
9. Liu, L.; Yao, Z.; Ye, Y.; Lin, Q.; Chen, S.; Zhang, Z.; Xiang, S. Enhanced Intrinsic Proton Conductivity of Metal–Organic Frameworks by Tuning the Degree of Interpenetration. *Cryst. Growth Des*. **2018**, *18*, 3724-3728.
10. Kim, S.; Joarder, B.; Hurd, J. A.; Zhang, J.; Dawson, K. W.; Gelfand, B. S.; Wong, N. E.; Shimizu, G. K. H. Achieving Superprotonic Conduction in Metal–Organic Frameworks through Iterative Design Advances. *J. Am. Chem. Soc*. **2018**, *140*, 1077-1082.
11. Dybtsev, D. N.; Ponomareva, V. G.; Aliev, S. B.; Chupakhin, A. P.; Gallyamov, M. R.; Moroz, K. N.; . Kolesov, B. A.; Kovalenko, K. A.; Shutova, E. S.; Fedin, V. P. High Proton Conductivity and Spectroscopic Investigations of Metal–Organic Framework Materials Impregnated by Strong Acids. *ACS Appl. Mater. Interfaces* **2014**, *6*, 5161-5167.
12. Tu, T. N.; Phan, N. Q.; Vu, T. T,; Nguyen, H. L.; Cordova, K. E.; Furukawa, H. J. High proton conductivity at low relative humidity in an anionic Fe-based metal–organic framework. *Mater. Chem. A* **2016**, *4*, 3638-3641.
13. Kim, S.; Dawson, K. W.; Gelfand, B. S.; Taylor, J. M.; Shimizu, G. K. H. Enhancing Proton Conduction in a Metal–Organic Framework by Isomorphous Ligand Replacement. *J. Am. Chem. Soc*. **2013**, *135*, 963-966.
14. Ramaswamy, P.; Wong, N. E.; Gelfand, B. S.; Shimizu, G. K. H. A Water Stable Magnesium MOF That Conducts Protons over 10^{-2} S cm^{-1}. *J. Am. Chem. Soc.* **2015**, *137*, 7640-7643.
15. Zhong, H.; Fu, Z. H.; Taylor, J. M.; Xu, G.; Wang, R. H. Covalent Organic Gels: Inorganic Acid-Impregnated Covalent Organic Gels as High-Performance Proton-Conductive Materials at Subzero Temperatures. *Adv. Funct. Mater*. **2017**, *27*, 1701465.
16. Borges, D. D.; Devautour-Vinot, S.; Jobic, H.; Ollivier, J.; Nouar, F.; Semino, R.; Devic, T.; Serre, C.; Paesani, F.; Maurin, G. Proton Transport in a Highly Conductive Porous Zirconium-Based Metal–Organic Framework: Molecular Insight. *Angew. Chem. Int. Ed.* **2016**, *55*, 3919-3924.
17. Ponomareva, V. G.; Kovalenko, K. A.; Chupakhin, A. P.; Dybtsev, D. N.; Shutova, E.S.; Fedin, V. P. Imparting High Proton Conductivity to a Metal–Organic Framework Material by Controlled Acid Impregnation. *J. Am. Chem. Soc.* **2012**, 134, 15640-15643.
18. Taylor, J. M.; Dawson, K. W.; Shimizu, G. K. H. A Water-Stable Metal–Organic Framework with Highly Acidic Pores for Proton-Conducting Applications. *J. Am. Chem. Soc.* **2013**, 135, 1193-1196.
19. Han, Y. H.; Ye, Y. X.; Tian, C. B.; Zhang, Z. J.; Du, S. W.; Xiang, S. C. High proton conductivity in an unprecedented anionic metalloring organic framework (MROF) containing novel metalloring clusters with the largest diameter. *J. Mater. Chem. A.* **2016**, 4, 18742-18746.

****